ANALYSIS OF CORONA-AFFECTED SURGE PROPAGATION ALONG MONOPOLAR TRANSMISSION LINES

by

Dragan V.Brankovic

A thesis
presented to the University of Manitoba
in partial fulfillment of the
requirements for the degree of
Master of Science
in
Department of Electrical Engineering

Winnipeg, Manitoba

ISBN 0-315-44133-X

ANALYSIS OF CORONA-AFFECTED SURGE PROPAGATION ALONG MONOPOLAR TRANSMISSION LINES

BY

DRAGAN V. BRANKOVIC

A thesis submitted to the Faculty of Graduate Studies of the University of Manitoba in partial fulfillment of the requirements of the degree of

MASTER OF SCIENCE

I hereby declare that I am the sole author of this thesis.

I authorize the University of Manitoba to lend this thesis to other institutions or individuals for the purpose of scholarly research.

Dragan V.Brankovic

I further authorize the University of Manitoba to reproduce this thesis by photocopying or by other means, in total or in part, at the request of other institutions or individuals for the purpose of scholarly research.

Dragan V.Brankovic

The University of Manitoba requires the signatures of all persons using or photocopying this thesis. Please sign below, and give address and date.

ABSTRACT

With the emergence of HVDC transmission, the studies of corona and its influence on attenuation and distortion of travelling waves became increasingly important. The practical significance of such studies is thet all HVDC transmission lines operate above corona onset voltage and that voltage surges on the line associated with either switching or lightning phenomena, are of even greater amplitude. Several good mathematical model for handling the problem of surge propagation on HVAC lines, taking corona into account, have been developed in the past. In this study, the performances of some of these models are compared and the most suitable one, from the point of view of accuracy and practical applicability, is implemented on a monopolar semi-infinite HVDC transmission line. The propagation of overvoltage surges along one pole of the Nelson River transmission line is simulated with a practical range of positive input voltage waveforms and the numerical procedure optimized. The results of the simulation are analyzed and their possible implication on the insulation co-ordination in HVDC transmission systems is indicated.

ACKNOWLEDGMENTS

I want to express my profound gratitude to Dr. I.M.R. Ciric and Dr. M.R.Raghuveer for their invaluable guidance through the course of this work.

My grateful acknowledgment is directed to Manitoba Hydro and NSERC for their partial funding this work.

My wife, Laura Brankovic, deserves special thanks for her help with stylization and editing of this text, as well as for her encouragement and understanding.

I also want to express my gratitude to my parents, Senka and Vojislav, and to my brother Milan, for their love and moral support during the years of my graduate studies at the University of Manitoba.

CONTENTS

ABSTRACT iv

ACKNOWLEDGMENTS v

Chapter page

1. INTRODUCTION 1

1.1 Transmission Line Corona 2
1.2 Transmission Line Equations (TLE) 10
1.3 Approaches to Corona Modelling 13
1.4 Numerical Methods 14
1.4.1 Frequency-Domain Based Technique 14
1.4.2 Time-Domain Based Methods 16
1.5 Scope of the Thesis 16

2. EXISTING MODELS 19

2.1 Literature Review 19
2.1.1 Single Shell Model (SSM) 20
2.1.2 Conductance Model 27
2.1.3 Approximate Q-V loop Model of C. Gary et al. 32
2.1.4 Frequency-Domain Q-V Loop Model 34
2.1.5 Approximate Q-V loop model of A.Inoue 42
2.2 Finite Difference Representation of TLE . . . 48

3. COMPARISONS 50

3.1 Application of the Finite Difference Method (FDM) 50
3.2 Comparison of Corona Models 52
3,3 Conclusion 65

4. CORONA MODEL IMPLEMENTATION ON HVDC TRANSMISSION LINES 67

4.1 Important Assumptions 67
4.2 Parameters of the Model 69
4.2.1 Transmission Line Inductance, L_o 69
4.2.2 Geometric Capacitance of the Line, C_o 70
4.2.3 Corona Inception Voltage, V_o 70
3.2.4 Dynamic Capacitance, C 72
3.2.5 Transmission Line Conductance, G 75

4.3 Parameters of the Line Used for Simulation 78
4.4 Description of the Waveforms Used for Simulation 81
4.5 Analysis of Numerical Accuracy 82
4.6 Description of Simulation Cases 87
4.7 Analysis of the Results of the Simulation . . 88
4.8 Description of the Program 98

5. CONCLUSION AND SUGGESTIONS FOR FURTHER RESEARCH . . 105

LIST OF REFERENCES 111

Appendix page

A. PROGRAM FOR THE SIMULATION OF CORONA-AFFECTED VOLTAGE SURGE PROPAGATION ALONG MONOPOLAR TRANSMISSION LINES 113

LIST OF TABLES

Table		page
2.1.	Line geometry and the modelling parameters used by Lee	30
2.2.	Geometric and electric line parameters used by Inoue	44
2.3.	Values of the empirical constants suggested by Inoue	44
2.4.	Key features of the reviewed models	46
2.5.	Key features of the examples used for numerical simulation with the reviewed models	47
3.1.	Comparison of the performances of EMTP and FDM in terms of the standard deviation for a lossless line subjected to a 1200 kV, 1.2/50 μs voltage impulse	52
3.2.	Comparison in terms of the standard deviation between voltages computed by different models and voltages experimentally obtained by Lee	57
3.3.	Comparison in terms of the standard deviation between voltages computed with different models and voltages experimentally obtained by Inoue	61
4.1.	Values of the bundling coefficient B^2	71
4.2.	Electrical parameters of a monopolar HVDC transmission line with the Nelson River conductor bundle configuration	79
4.3.	Values of empirical corona loss constants σ_1 and σ_2 for positive voltage impulses, a fair weather condition and the Nelson River conductor bundle configuration	80
4.4.	Parameters of the input waveforms	82

4.5. Numerical errors caused by variation of time and displacement steps 85

4.6. Computed attenuation of a full 450 kV, 1.2/50 μs positive voltage impulse 91

4.7. Computed attenuation of a 450 kV, 1.2/50 μs positive voltage impulse chopped on the front 92

4.8. Computed attenuation of a 450 kV, 1.2/50 μs positive voltage impulse chopped at the tail 93

4.9. Computed attenuation of a 450 kV, 250/2500 positive voltage impulse 94

4.10. Computed attenuation of a full 450 kV, 1.2/50 μs positive voltage impulse 95

4.11. computed attenuation of a 450 kV, 1.2/50 μs positive voltage impulse chopped on the front 96

4.12. Computed attenuation of a positive 450 kV, 1.2/50 μs chopped at the tail 97

LIST OF FIGURES

Figure		page
1.1.	Charge disposition around a conductor in corona	5
1.2.	Steady-state Q-V characteristics	6
1.3.	Typical impulse corona Q-V characteristic	8
1.4.	Waveform decomposition into levels	15
2.1.	A typical Q-V characteristic generated by SSM	24
2.2.	Representation of transmission line sections in the SSM	25
2.3.	A typical single-valued Q-V characteristic used in the conductance model	29
2.4.	Representation of a transmission line section in the conductance model	31
2.5.	A typical Q-V loop used in the approximate Q-V loop model of Gary et al.	33
2.6.	Geometry of a coronating conductor used in the frequency-domain Q-V loop model	35
2.7.	Simplified Q-V characteristics used in the frequency-domain Q-V loop model	38
2.8.	Resistive element R used in the frequency-domain Q-V loop model to account for corona	40
2.9.	A simplified Q-V characteristic used in the approximate Q-V loop model of Inoue	43
3.1.	Input waveform used by Lee	57
3.2.	Comparison between waveforms computed by the conductance model[10] and experimental waveforms obtained by Lee	58
3.3.	Comparison between waveforms computed by the Q-V loop model[14] and experimental waveforms obtained by Lee	59

3.4. Comparison between waveforms computed by the approximate Q-V loop model[11] and experimental waveforms obtained by Lee 60

3.5. Input waveform used by Inoue 61

3.6. Comparison between waveforms computed by the conductance model[10] and experimental waveforms obtained by Inoue 62

3.7. Comparison between waveforms computed by the Q-V loop model[14] and experimental waveforms obtained by Inoue 63

3.8. Comparison between waveforms computed by the approximate Q-V loop model[11] and experimental waveforms obtained by Inoue . . . 64

4.1. Dynamic capacitance v.s. applied voltage for the Nelson River conductor bundle configuration. Fair weather conditions. Positive voltage impulse. Non-energized line. 74

4.2. Conductance v.s. applied voltage for the Nelson River conductor bundle configuration. Fair weather condition. Positive voltage impulse. Non-energized line. 77

4.3. Nelson River conductor bundle geometry 78

4.4. Influence of different values of Δt and Δx on V_0 . a) base waveform. b) Δt=0.02 μs, Δx=0.02 km. 84

4.5. Propagation of a positive 450 kV, 1.2/50 μs voltage impulse along the line energized with 450kV. a) 0 km, b) 0.6 km, c) 1.2 km, d) 2.4 km 91

4.6. Propagation of a 450 kV, 1.2/50 μs positive voltage impulse chopped at the front, along the line energized with 450 kV. a) 0 km, b) 0.6 km, c) 1.2 km, d) 2.4 km 92

4.7. Propagation of a 450 kV, 1.2/50 μs positive voltage impulse chopped at the tail, along the line energized with 450 kV. a) 0 km, b) 0.6 km, c) 1.2 km, d) 2.4 km 93

4.8. Propagation of a 450 kV, 250/2500 μs positive voltage impulse along the line energized with 450 kV. a) 0 km, b) 60 km, c) 120 km, d) 240 km 94

4.9. Propagation of a positive 450 kV, 1.2/50 μs voltage impulse along the non-energized line. a) 0 km, b) 0.6 km, c) 1.2 km, d) 2.4 km. V_0 =318 kV. 95

4.10. Propagation of a 450 kV, 1.2/50 μs positive voltage impulse chopped at the front, along the non-energized line. a) 0 km, b) 0.6 km, c) 1.2 km, d) 2.4 km. V_0 = 318 kV 96

4.11. Propagation of a 450 kV, 1.2/50 μs positive voltage impulse chopped at the tail, along the non-energized line. a) 0 km, b) 0.6 km, c) 1.2 km, d) 2.4 km. V_0 = 318 kV. 97

4.12. Flowchart of the main program 99

1. INTRODUCTION

Power systems are subjected to two types of overvoltage surges. They are classified, according to their origin as lightning or switching surges. Lightning surges can be direct or indirect. They are characterized by a very short rise-time (in the order of a microsecond), high amplitude, and relatively short duration. Switching surges are caused by switching of a circuit either to clear the fault or as a normal operating procedure. They have a much longer rise-time (in the order of a few hundreds microseconds) and decay more slowly. Switching surges are of prime importance in the determination of insulation levels in EHV, UHV, and HVDC transmission systems.

The effect of an overvoltage surge on a piece of equipment is dependent on the waveform of the surge impressed upon the piece of equipment. This waveform is usually different from the waveform at the point of injection into the system. The modifications are caused by attenuation, distortion, and reflections of the overvoltage wave as it travels from the point of its origin to the point of interest.

It is evident that for a better evaluation of the effects of overvoltage surges at different points in a power system, it is necessary to take into consideration as many

effects as possible which affect the propagation and change the shape of the overvoltages. This study focusses on the influence of the corona effect on overvoltage surges propagating along HVDC transmission lines.

1.1 Transmission Line Corona

Transmission line corona has been studied since almost the beginning of this century. F.W. Peek was the foremost pioneer in this area and his work[1] resulted in the empirical expressions for corona losses and corona inception voltage, expressions that are in use even today. His work was followed by that of many researchers. In 1924, Ryan and Henline explained the hysteresis character of corona.[5] In 1937, Skilling and Dykes published experimental results[6] showing the influence of corona on the distortion of travelling overvoltage waves. Since then, due to an increase in the operating voltage of AC transmission lines and the emergence of HVDC transmission, studies of corona and its effects have become increasingly important.

Transmission line corona is a self-sustained partial breakdown of the air around a high voltage conductor where the electrical field is non-uniform. Corona can be established around a conductor of either positive or negative polarity. Although the ionization process differs in these two cases, the resulting effect is similar - a space charge of like polarity is inserted into the surrounding space, and moves away from the conductor. When

the conductor is energized with alternating voltage, the periodic reversals of polarity prevent the space charge from leaving the vicinity of the conductor. Corona can be established under steady-state conditions (steady-state corona), or be initiated by an overvoltage surge. In both cases, the instantaneous value of the applied voltage must be higher than a critical value, known in the literature as the corona inception voltage. This value depends on conductor bundle geometry, conductor surface condition, atmospheric pressure, air humidity, etc. Corona initiated by an overvoltage surge has a unipolar character and it is known in the literature as impulse corona.

The space around a conductor in corona can be divided into two zones, the ionization zone and the interelectrode zone. The ionization zone is defined[9] as the space around the high voltage conductor where the resultant electrical field is strong enough so that the first Townsend coefficient of ionization exceeds the coefficient of attachment. In this zone, electrons are released from the atoms of the air and accelerated towards or away from the conductor, depending on its polarity. Collisions between fast electrons and atoms of the air result in additional electrons in an avalanche process. The interelectrode zone is considered to be the space between the boundary of the ionization zone and adjacent conductors, or between the boundary and the ground. In this zone, the attachment coefficient is larger then the first Townsend coefficient of

ionization. In the case of unipolar corona, the interelectrode zone consists primarily of ions of the same polarity as the conductor, forming a space charge which migrates away from the conductor, deeper into the interelectrode space. The formation of the two zones and the different types of charges will be explained by means of Fig.1.1 using an example of a conductor in steady-state DC corona.

Fig.1.1.a represents the case of a positive conductor in corona. As long as the voltage is below the corona inception voltage, V_0, the charge on the conductor surface changes proportionally with the applied conductor voltage; the constant of proportionality is the geometric capacitance of the line per unit length, C_0, i.e.:

$$Q = C_0 V \qquad \ldots\ldots(1.1)$$

In this case, no space charge exists as the air is not ionized. Once the inception voltage is exceeded, the air around the conductor becomes ionized. In an avalanche process, positive ions are created by the electrons which are readily attracted by the conductor and neutralized at its surface by an equal positive charge supplied from the source. Positive ions, which are left behind, slowly migrate away from the conductor. As the mobility of the electrons is much higher than that of the positive ions, the neutralization of the electrons is a much faster process

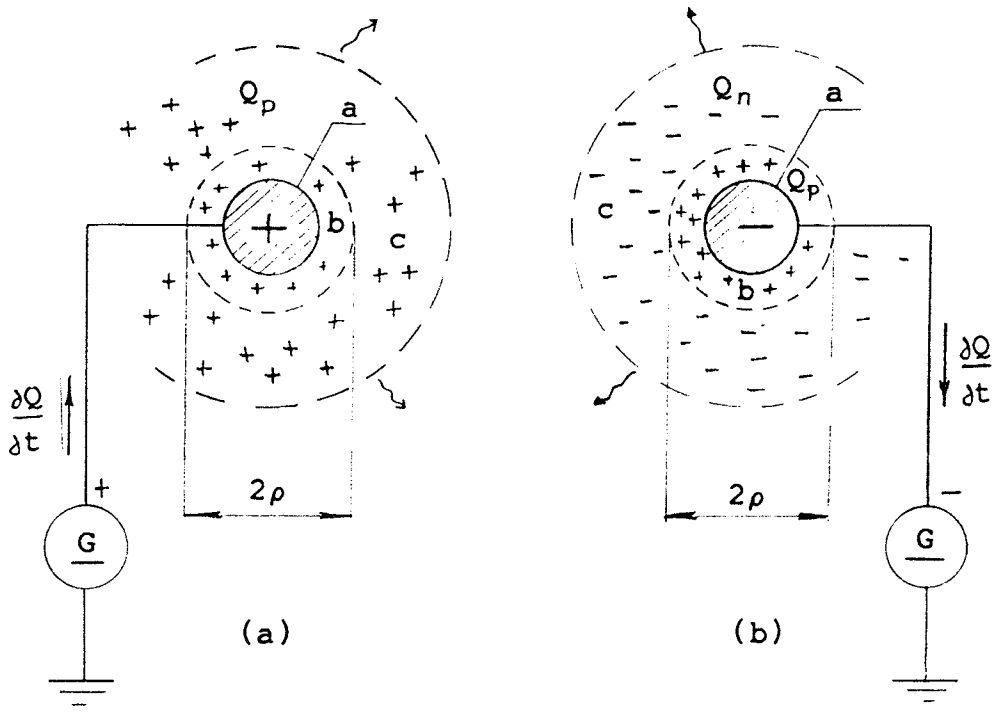

a - conductor
b - ionization zone
c - interelectrode zone
Q - total charge per unit length supplied from the source
Q_p - positive space charge per unit length
Q_n - negative space charge per unit length
ρ - radius of the ionization zone

Figure 1.1: Charge disposition around a conductor in corona

than the movement of the ions. Therefore, it can be considered that the electric field around the conductor is affected only by the positive space charge, Q_p, dominating in both the ionization and the interelectrode zone. The

relationship between the charge supplied by the source, Q, and the applied voltage, in this case, is shown in Fig. 1.2.a. It can be noted that for different values of steady-state voltage above the inception value, the charge Q increases at a rate much higher than that before corona

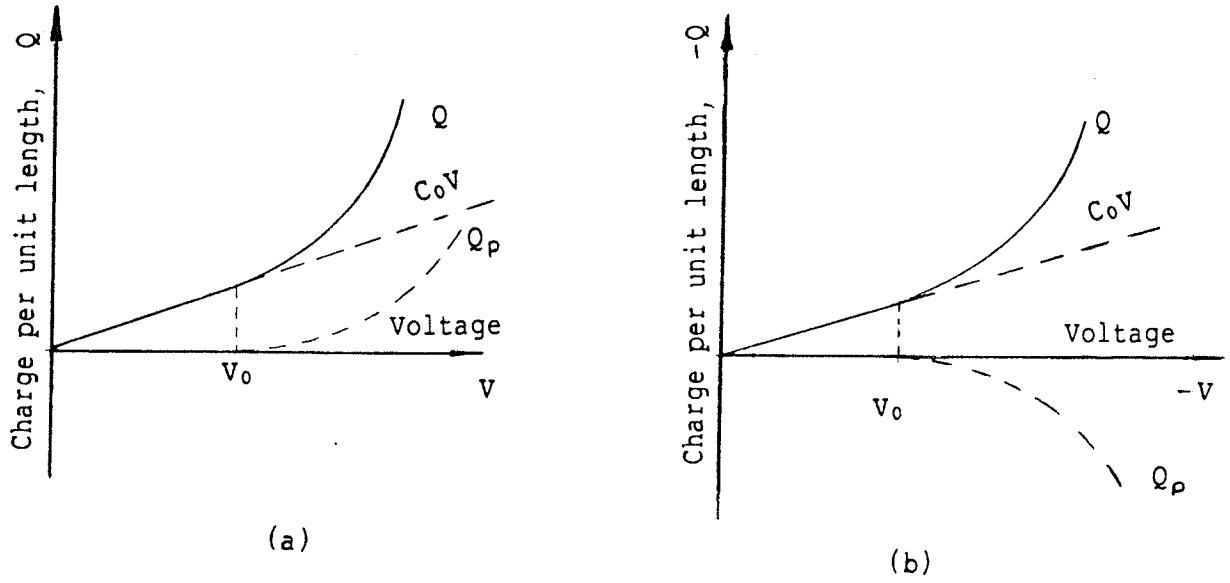

Figure 1.2: Steady-state Q-V characteristics

initiation.

An example of a negative conductor in corona is shown in Fig.1.2.b. When the voltage is below the inception value V_0, the relationship between the charge supplied from the source and the voltage is the same as that described by expression (1.1). When the inception voltage is exceeded, the air around the conductor becomes ionized.

New electrons, created in an avalanche process, move away from the conductor leaving the positive ions to be attracted by the conductor and neutralized. The electrons move up to the boundary where ionization and attachment are equally probable. Beyond this boundary they are captured by the neutral atoms of the air, forming negative ions. These processes result in a positive space charge, Q_+, dominating in the ionization zone, and in a negative space charge, Q_-, dominating in the interelectrode zone. The space charge from the ionization zone is attracted by the conductor and neutralized at its surface by an equal negative charge which is supplied from the source. The neutralization process causes the charge Q to increase at a much higher rate than that defined by Eq.(1.1). The Q-V relationship, in this case, is shown in Fig.1.2.b for different values of steady-state voltage. It should be noted that this relationship shows the same form of nonlinearity as in the previous case.

Experimental results[8] as well as the experience of several researchers[9,15] indicate that the charge neutralized at the conductor surface ($-Q_+$) is voltage-dependent. The magnitude of this charge increases nonlinearly with the applied voltage.

Under steady-state conditions, the radius of the ionization zone as well as the value of the space charge are time invariant. In the case of impulse corona, however,

these values which are functions of voltage, become functions of time. Experiments[8] have shown that, in the case when the applied conductor voltage has the form of an impulse, the Q-V characteristic has the form of a loop, for

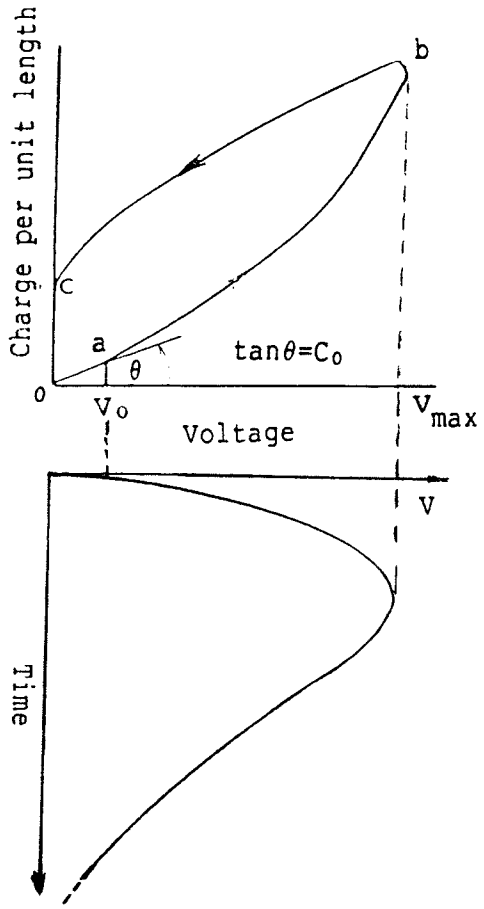

Figure 1.3: Typical impulse corona Q-V characteristic

both positive and negative voltage impulses(Fig. 1.3).

Section o-a on the Q-V loop in Fig.1.3 is linear and corresponds to non-corona conditions. The charge Q

increases proportionally to the applied voltage according to Eq.(1.1), as long as the voltage is below V_0 . Section a-b of the loop corresponds to corona conditions where $V>V_0$ and $V/t>0$. Under these conditions, an additional charge of the same polarity as the conductor is supplied from the source to neutralize the space charge which is in contact with the conductor surface. Point b on the loop (Fig.1.3), corresponds to the maximum instantaneous value of the applied voltage. From this point on, as the voltage decreases, the space charge around the conductor remains almost constant which cause the total charge in the ionized region, Q, to change almost linearly with the voltage. Section b-c of the Q-V loop represents the conditions when V<V and $V/t<0$. Experimental results[8] show that the return slope of the Q-V loop is almost equal to that of section o-a. If the voltage decays very slowly, the space charge eventually disperses due to diffusion which causes a curving of the return slope of the Q-V loop. Section o-c in Fig.1.3 represents the value of the space charge generated during impulse corona after the applied voltage is decreased to zero. This space charge migrates away from the conductor in the process of diffusion until it reaches the distance where its influence on the electric field around the conductor is negligible.

Although the radius of the ionization zone varies with voltage, its thickness is negligible in comparison with the

radius of the conductor. Hence, it is often assumed in the literature that even in the case of impulse applied voltage, the interelectrode zone starts from the surface of the conductor and that the conductor gradient is maintained constant at a value of E_o, for all voltages greater than the inception value (Kaptzov).

1.2 Transmission Line Equations (TLE)

The response of a transmission line, neglecting corona and the skin effect, can be represented by a system of two linear partial differential equations known as Transmission Line Equations (TLE), i.e.:

$$-\partial I/\partial x = C_o\ (\partial V/\partial t) + G_o V \qquad .....(1.2.a)$$

$$-\partial V/\partial x = L_o\ (\partial I/\partial t) + R_o I \qquad .....(1.2.b)$$

where:

V = instantaneous value of voltage,

I = instantaneous value of current,

C_o = geometric capacitance of the line per unit length,

L_o = self inductance of the line per unit length,

R_o = resistance of the line per unit length,

G_o = conductance of the line per unit length,

t = time variable,

and x = distance from the location of excitation

Eqs.(1.3.a) and (1.3.b) are linear because the parameters C_0, L_0, R_0, and G_0 are constant. When the transmission line is not in corona, the conductance G_0 is very small and it is usually neglected. However, when the line operates in corona, both the line capacitance and the conductance become nonlinear functions of the conductor voltage.

Furthermore, when the line is subjected to fast transients such as lightning surges, in addition to corona, the skin effect contributes to the attenuation and distortion of the transient response. Since the corona effect is reflected in the voltage-dependent line capacitance and line conductance, and the skin effect in the frequency dependent line resistance, these two phenomena do not interact with each other and therefore can be studied independently.

According to the results[8,9,11,15] available in the literature, the corona effect can be represented accurately enough by assuming that the total charge supplied by the source per unit length, Q, depends on both the magnitude V and the rate of rise $\partial V/\partial t$ of the applied voltage, i.e.:

$$Q=Q(V,\partial V/\partial t)$$

In order to take the corona effect into account, the system of equations (1.3) can be written in the following form:

$$-\partial I/\partial x=(\partial Q/\partial V)(\partial V/\partial t) \qquad .....(1.3.a)$$

$$-\partial V/\partial x=L_o\ (\partial I/\partial t) + R_o I \qquad .....(1.3.b)$$

The coefficient $\partial Q/\partial V$ is called the dynamic capacitance of the line, C_d, and represents the slope on the appropriate Q-V characteristic. Thus, the TLE in Eqs.(1.3), may be written as:

$$-\partial I/\partial x=C_d\,(\partial V/\partial t) \qquad .....(1.4.a)$$

$$-\partial V/\partial x=L_o\ (\partial I/\partial t)+R_o I \qquad .....(1.4.b)$$

It should be noted that C_d depends not only on the voltage amplitude, but also on rate of rise of the applied voltage, i.e.:

$$C_d = C_d\,(V, \partial V/\partial t)$$

In other words, the Q-V characteristics are different for different types of surges. Field measurements[8] indicate that Q-V loops are narrower for steeper surges.

It should also be noted that the conductance term is omitted from Eqs.(1.3). This is justified by the fact that the area enclosed by a Q-V loop is proportional to corona losses and therefore no additional parameter is needed to account for these losses.

1.3 Approaches to Corona Modelling

There are two basic approaches to model impulse corona.

One approach is based on an analytical approximation of the Q-V characteristics, which is usually done piecewise. The TLE, in this case, have the form of Eqs.(1.4), and are solved with C_d taken as the slope on the approximate Q-V characteristic. The main disadvantage of this approach is the very limited practical applicability of the model since the Q-V characteristics are available only for those classes of voltage waveforms which are easily generated under laboratory conditions.

The other approach is based on the analytical approximation of that portion of the Q-V characteristic which has a positive first derivative. This approximation results in a single-valued Q-V characteristic. Corona losses, however, are accommodated by an appropriately defined conductance term G(V) derived from consideration of either Peek's or Popkov's corona loss laws which are valid in the steady state. Therefore, the TLE in this case have the following form:

$$-\partial I/\partial x = C_d\,(\partial V/\partial t) + G(V)V \qquad .....(1.5.a)$$

$$-\partial I/\partial t = L_o\,(\partial I/\partial t) + R_o I \qquad .....(1.5.b)$$

The expressions for C_d and G are both nonlinear functions of the applied voltage.

A detailed description of models based on each of the above approaches, as well as a comparison of results obtained by application of each model to a practical transmission line geometry, is included in Chapter 2.

1.4 Numerical Methods

Once a particular approach to corona modelling is chosen and its parameters defined, an appropriate numerical method for solving the nonlinear TLE remains to be chosen. This section discusses some numerical techniques that may be used:

1.4.1 Frequency-Domain Based Technique

In the frequency-domain, it is very convenient to use a Fourier Series or, more preferably, a Fast Fourier Series based method. It is assumed that all the parameters in the TLE have constant values associated with each harmonic considered.

The corresponding wave propagating along positive x-direction has the following form:

$$V_2\ (x,t)=V_m\,[\exp(-\alpha x)]\cos(\omega t-\beta x) \qquad .....(1.6)$$

where:

α - attenuation coefficient,

β - phase constant,

ω - angular frequency,

V_m - maximum value of voltage.

Since some parameters in the equations are nonlinear functions of voltage, it is necessary to obtain the solution for several voltage ranges above the corona inception voltage, using different but constant voltage-dependent parameters within each range. The original input waveform

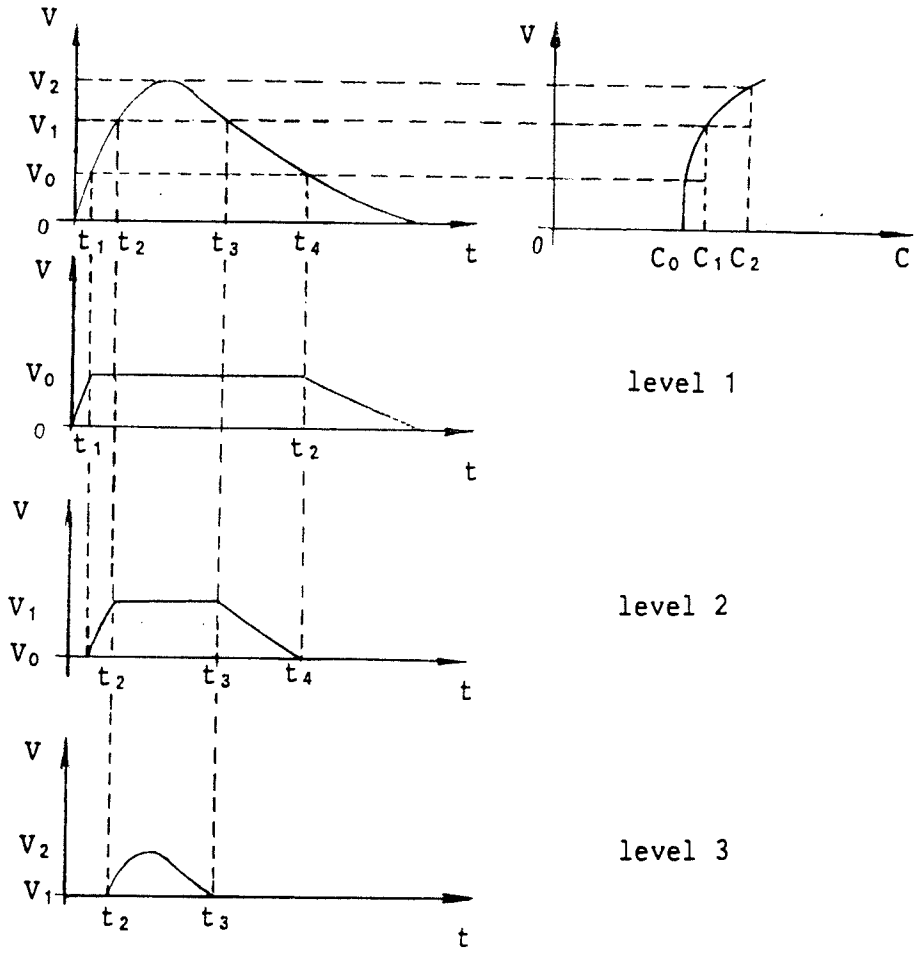

Figure 1.4: Waveform decomposition into levels

is decomposed into sub-waveforms, each of them corresponding to a particular voltage range, Fig.1.4, and a transient response of the line is found using each of the

sub-waveforms as an input waveform. A superposition of these solutions yields the solution to the original problem for given time and displacement.

It is apparent that the accuracy of the final solution depends on the number of voltage levels above the corona inception voltage. The advantage of this method is that it is very convenient for considering frequency-dependent phenomena such as skin effect.

1.4.2 Time-Domain Based Methods

Time-domain based methods are more convenient for dealing with the nonlinear voltage dependent problems only and distributed transmission line parameters. The TLE given by Eqs.(1.5) can be solved by the Finite Difference Method where the partial differential equations are replaced with their finite difference representations.

1.5 Scope of the Thesis

This study focusses on the attenuating and distorting effect of corona on overvoltage waves travelling along monopolar single and multiconductor HVDC transmission lines. Several corona models developed for application on AC transmission lines will be reviewed in Chapter 2. The performances of several of those models will be compared in Chapter 3 and the results presented in this chapter serve as a basis for corona model implementation in HVDC transmission systems.

The application of the Finite Difference Method for modelling purposes in this study is also justified in this chapter.

The analysis of skin effect and its influence on attenuation and distortion of travelling overvoltage waves in HVDC transmission systems is not included in this study. It should be noted that corona and skin effects are phenomena that do not interact with each other. It is possible, therefore, to exclude the skin effect from the analysis without affecting the modelling of corona.

The implementation of a corona model in an HVDC transmission system is performed in Chapter 4. Distortion and attenuation of different types of overvoltage surges propagating along one pole of the Nelson River DC transmission line are analyzed, including the case when an overvoltage surge is superimposed on DC steady-state voltage. A description of the program used for the simulation is also given in this chapter.

The corona modelling in this study is performed in time-domain for the reasons explained in section 1.4.2. As a numerical technique, the Finite Difference Method is used.

The influence that corona has on attenuation and distortion of overvoltage surges travelling along a monopolar HVDC transmission line is analyzed and its possible implications on the insulation co-ordination in

HVDC transmission systems indicated in Chapter 5 of this thesis. The thesis is concluded by giving several suggestions for further research in this area.

2. EXISTING MODELS

The propagation of overvoltage waves along single and multiconductor transmission lines including the corona effect has been studied extensively, and different modelling techniques and computer programs have been developed. Most of the studies have focussed either on impulse corona on HVAC lines or steady state corona on HVDC lines.

In this chapter, several existing models are reviewed. Based upon a comparison study, the results presented in this chapter serve as a basis for corona model implementation on HVDC lines.

2.1 Literature Review

The transient behaviour of coronating HVAC or HVDC transmission lines may be described by the set of TLE, Eqs.(1.5), with corona taken into account by means of nonlinear transmission line parameters, as described in section 1.3.

In the past ten years several good models for handling the problem of surge propagation on HVAC lines, taking corona into account, have been developed. These models differ from each other in the approach adopted to model corona and the numerical methods that have been used to

solve the system of TLE. In this section, five of these models are reviewed.

2.1.1 Single Shell Model (SSM)

This model has been proposed by M. Afghani and R.J. Harrington[9] and employs what the authors call the "single shell method". It represents a simplified version of the multishell model applicable for the analysis of AC steady-state corona developed by the same authors. The simplified version is applicable for analyses involving the propagation of lightning and switching overvoltage surges along HVAC transmission lines. In this model, corona is simulated by means of Q-V characteristics. However, what makes this model distinct from other models based upon the use of the Q-V characteristics for modelling corona is that, in this case, the Q-V characteristics are numerically generated by the model. The characteristics are used thereafter for evaluating the appropriate voltage-dependent nonlinear transmission line parameters.

For modelling the system of the coronating conductor and the surrounding space charge, the authors assume that the space charge is situated concentrically around the conductor; their analysis is based on the following assumptions:

1. The ionization zone is neglected which implies that, for both the positive and negative conductor in

corona, the space charge consists of ions of the same polarity as the conductor.

2. The space charge emitted by the conductor in corona is concentrated within a thin shell of a radius ρ, concentric with the conductor.
3. The total charge in the ionized regions is the sum of:
   a) the space charge emitted by the conductor
   b) the charge bound on the conductor surface, which is assumed to be constant and equal to the inception value Q_o as long as corona exists
   c) the charge returned to the conductor from the space charge, either due to an alternating applied voltage, or due to a reversal of polarity of an overvoltage surge.
4. Half the magnitude of the total space charge contributes to the electric field which controls the movement of the shell.

The Q-V characteristics are generated through the following iterative procedure:

As long as the applied voltage is below the inception value V_o, the charge bound on the conductor surface is represented as:

$$Q_j = C_o V_j = C_o\ V(t_j), \quad j=1,\ldots,n \qquad .....(2.1)$$

where:

C_0 = geometric capacitance of the line

V_j = applied voltage at the point of time $t_j = j\ \Delta t$

Δt = a time step

The value of the inception voltage V_0 is determined from Peek's expression for the inception voltage gradient.[1]

Assume that at time t_k , $k<n$, the applied voltage exceeds the inception voltage V_0 . In this case, a shell with the space charge:

$$Q_k^s = C_0 V_k - Q_0 \qquad .....(2.2)$$

emerges from the conductor. The radius of the shell is found from the following two equations:

$$r_k = a + \Delta r_k \qquad .....(2.3)$$

$$\Delta r_k = \mu E_0\ \Delta t \qquad .....(2.4)$$

where:

a = equivalent (GMR) radius of a conductor bundle

μ = mobility of the ions that the space charge consists of.

This space charge induces on the conductor surface charge Q which is taken into account in the subsequent time step as an algebraic value.

$$Q_k^i = -Q_k^s \ln(r_k/a) = -(C_0 V_k - Q_0)\ \ln(r_k/a) \qquad .....(2.5)$$

The total charge supplied by the source at this point is obtained by addition of the total charge bound on the conductor surface, and the space charge Q_k^s, i.e.:

$$Q_k = Q_o + Q_k^s - Q_{k-1}^i \qquad \text{.....(2.6)}$$

where Q_{k-1}^i is equal to zero. Using the fourth assumption, the electrical field which controls the movement of the shell, is evaluated as:

$$E_k = (1/2\pi\epsilon_o)(C_o V_k + Q_k^s/2) \qquad \text{.....(2.7)}$$

In the subsequent time step, a new value of the shell radius is obtained from:

$$r_{k+1} = r_k + \Delta r_k$$
$$\Delta r_k = \mu E_k \Delta t$$

The new value of the space charge is equal to the difference between the total charge bound on the conductor surface and Q_o, i.e.

$$Q_{k+1}^s = C_o V_{k+1} - Q_o \qquad \text{.....(2.8)}$$

The induced charge due to the new space charge is obtained as:

$$Q_{k+1}^i = -Q_{k+1}^s \ln(r_{k+1}/a) \qquad \text{.....(2.9)}$$

and the total charge in the ionized region as:

$$Q_{k+1} = Q_o + Q_{k+1}^s - Q_k^i$$

The step is concluded by the calculation of the electrical field at the radius r_{k+1} , as:

$$E_{k+1}=(1/2\pi\epsilon_0 r_{k+1})(C_0V_{k+1}+Q^s_{k+1}/2)$$

The Q-V characteristic generated by the model represents the relationship between the total charge in the ionized region, Q, and the applied voltage, V; a typical Q-V

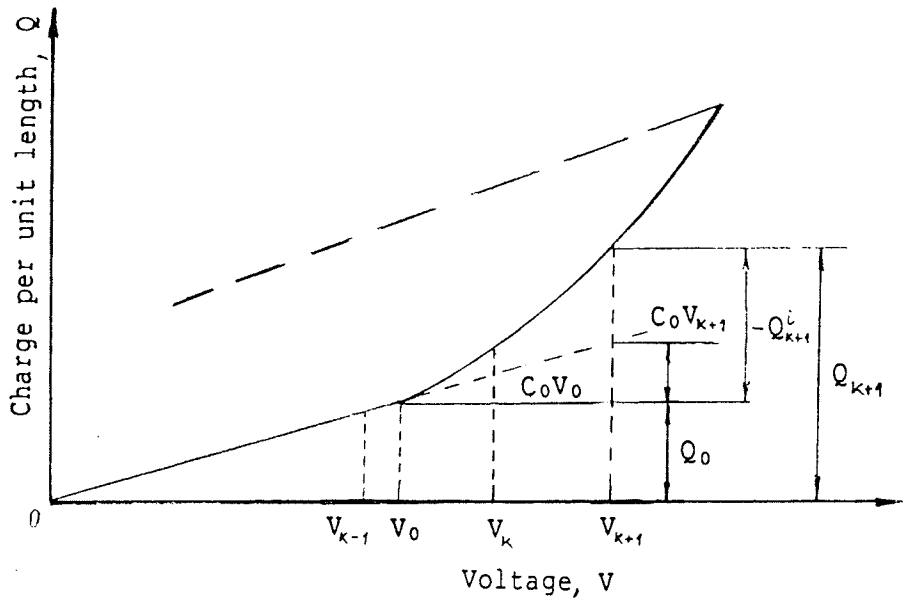

Figure 2.1: A typical Q-V characteristic generated by SSM

characteristic generated by this model is shown in Fig.2.1.

In the case of semi-infinite transmission lines, when distortion and attenuation of overvoltage surges without multiple peaks have to be calculated, the authors suggest the use of linearized Q-V characteristics with C expressed in the following form:

$$C_d = \begin{cases} C_0, & V<V_0,\ \partial V/\partial t>0 \quad .....(2.10.a) \\ C_0 + \Delta C, & V_0<V<V_m,\ \partial V/\partial t>0 \quad .....(2.10.b) \\ C_0, & 0<V<V_m,\ \partial V/\partial t>0 \quad .....(2.10.c) \end{cases}$$

The Q-V characteristic generated in this model is used to define an appropriate current source I_{cor} which is actually a function of the nonlinear line capacitance and the line conductance. The transmission line is sectionalized and the current source lumped between two adjacent sections and ground, Fig.2.2. The length of the sections varies in the range of 30-400m, depending on the rate of rise of the

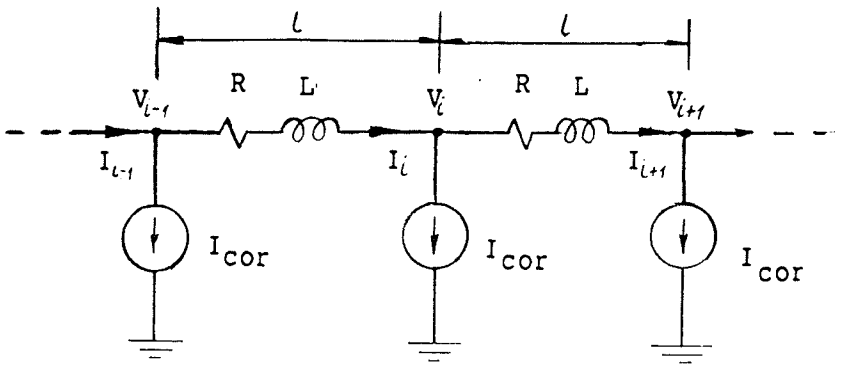

Figure 2.2: Representation of transmission line sections in the SSM

voltage impulses used in the simulation.

Consequently, the transient response of a coronating transmission line is found in the time-domain by solving the following set of partial differential equations:

$$(\partial^2/\partial x^2)\ \overline{V}(x,t)=[Z][Y]\ \overline{V}(x,t) \qquad .....(2.11.a)$$

$$(\partial/\partial x)\ \overline{I}(x,t)=-[Z]\ \overline{I}(x,t) \qquad .....(2.11.b)$$

written for each section and the conditions at the interface of any two adjacent sections (i and i+1, for example):

$$\overline{V_i}\ (l,t)=\overline{V}_{i+1}(0,t) \qquad .....(2.12.a)$$

$$\overline{I_i}\ (l,t)-\overline{I}_{i+1}(0,t)=\overline{I}_{cor} \qquad .....(2.12.b)$$

where:

x =distance along the line

l =length of the section

t =time from the beginning of the voltage impulse application at the beginning of the line

$\overline{V}$ =voltage vector

$\overline{I}$ =vector of the current

[Z] =series impedance matrix per unit length

[Y] =shunt admittance matrix per unit length

The authors analyzed the propagation of both lightning and switching positive voltage impulses along single and 4-conductor bundle transmission lines. The crest values of the voltage impulses in their examples ranged from 390 kV to

950 kV. It should be noted that the SSM generates Q-V characteristics which are dependent on the rate of rise of the voltage impulses. Therefore, the propagation of the voltage impulses is also affected by their steepness which is in agreement with the experimental measurements.[8,13] However, some limitations are inherent in this model. In the cases where the input voltage impulses do not exhibit oscillatory character, the ionized region (a shell in this model) continues to expand. Since the propagation time on long transmission lines can be relatively large, the assumption of cylindrical geometry is soon violated, which limits the propagation distances for simulating non-oscillatory transient conditions on transmission lines.

2.1.2 Conductance Model

This model is proposed by K.C. Lee,[10] and is based on a time-domain solution to the system of TLE given by Eqs. (1.5) with line resistance neglected. Corona is introduced by the nonlinear parameters C_d and G which are modelled as nonlinear functions of the applied voltage.

The dynamic capacitance in this model is defined by

$$C_d = C_0, \qquad V<V_0 \qquad .....(2.13.a)$$

$$C_d = C_0 + 2k_1\,(1-V_0/V\,), \qquad V>V_0 \qquad .....(2.13.b)$$

where:

$$k_1 = \sigma_1\sqrt{(ah)/2} \quad \times 10^{-8} \quad [F/km],$$

σ_1 = an empirically derived corona loss constant, [dimensionless],

a = equivalent radius (GMR) of a conductor bundle [m],

h = average suspension height [m],

C_0 = geometric capacitance of the line [F/km],

V_0 = corona inception voltage [kV].

Corona losses, however, are introduced by means of the conductance term, G, defined as:

$$G = k_2 (1-V_0/V)^2 \qquad .....(2.14)$$

where:

$k_2 = \sigma_2\sqrt{(ah)/2} \times 10^{-8}$ [S/km],

σ_2 = another empirically derived corona loss constant, [dimensionless]

Parameters σ_1 and σ_2 are derived empirically for a single-conductor and a 4-conductor bundle configurations by comparison of numerical and field measurements for these configurations under application of both positive and negative lightning-type voltage impulses. In the examples that the author used for simulation, the applied voltage impulses had the crest value of about 1500 kV and were taken from experimental measurements.

It should be noted that the Q-V characteristic in this model does not have the form of a loop. Such characteristic

is shown in Fig.2.3 and represents an analytical approximation of the part of an actual Q-V characteristic,

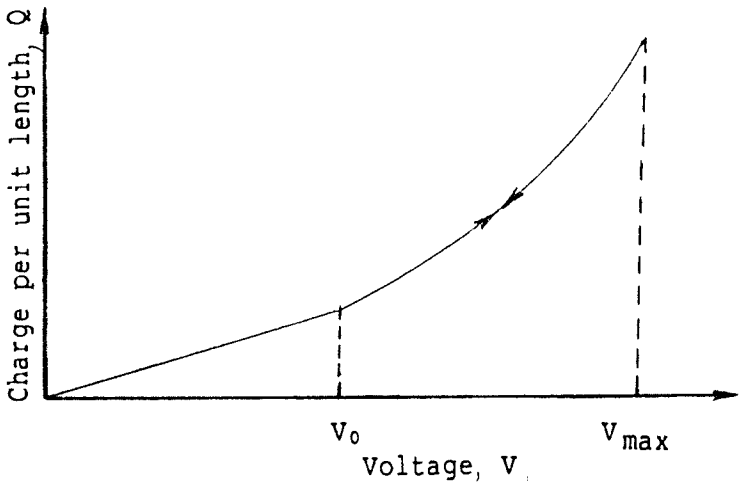

Figure 2.3: A typical single-valued Q-V characteristic used in the conductance model

where the first derivative is positive.

The characteristic in Fig. 2.3 is obtained by defining its slope, i.e. the dynamic capacitance, according to Eq.(2.13). Since the characteristic is single-valued, corona losses are introduced by another nonlinear parameter, i.e. conductance G defined in Eq.(2.14). The values of the modelling parameters proposed by the author are given in Tab.2.1.

TABLE 2.1

Line geometry and the modelling parameters used by Lee

constant	single cond.	4-cond.bundle
V_0 [kV]	277	558
positive impulse negative impulse	30 --	30 15
positive impulse negative impulse	10^7 --	$2x10^6$ 10^7
a [cm]	1.265	1.12
h [m]	22.200	14.00

The transmission line under consideration is divided into sections and the voltage dependent elements are lumped at the end of each section (Fig.2.4). A section length of 70m was found by the author to be the optimal length.

The solution to the problem is obtained in two steps. First, for each section, the solution is obtained by Bergeron's travelling wave technique without taking the nonlinear elements into account, yielding a Thevenin's equivalent for the linear part of the section. In the second step, the nonlinear elements are taken into account by applying the trapezoidal rule of linear interpolation. This procedure yields the values of the voltage and the current at the end of each section which are used as the input data for the next section.

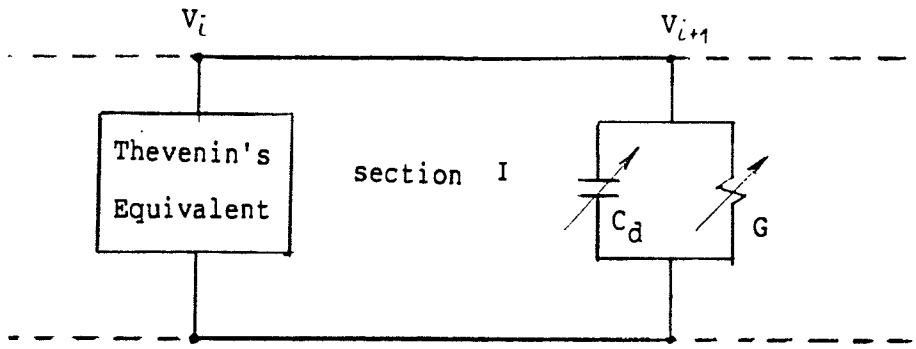

Figure 2.4: Representation of a transmission line section in the conductance model

It should be noted that the values of constants σ_1 and σ_2 depend on conductor bundle configuration, polarity and shape of a voltage impulse. A weakness of the model is that these constants can only be determined empirically, by comparison of numerically computed voltages with those obtained from field measurements. However, this is not a serious disadvantage because it is relatively easy to optimize a model with two adjustable parameters upon availability of experimental measurements.

2.1.3 Approximate Q-V loop Model of C. Gary et.al.

This model[11] includes both the corona and skin effects. The model is based on the time-domain solution of the system of TLE which has the following form:

$$-\partial I/\partial x = C_d\ (\partial V/\partial t) + G\ V \qquad .....(2.15.a)$$

$$-\partial V/\partial x = L_o\ (\partial I/\partial t) + (\partial/\partial t)\int_0^t R(t-t')I(x,t')dt' \qquad ..(2.15.b)$$

The skin effect is accounted for by means of the time(frequency)-dependent line resistance, R(t), which includes the resistances of the conductor and the ground return.

The authors replaced experimentally obtained Q-V characteristics with a simplified empirically developed one, Fig.2.5. The simplified characteristic was obtained after numerous laboratory experiments. The model was tested in the example of a 225 kV single-conductor line with the earth conductivity varied in the range from 0.015 S/m to 0.007 S/m. At the beginning of the line, different forms of positive lightning-type voltage impulses, with a crest value of 1120 kV, were applied. The line considered by the authors was assumed to be non-energized.

The dynamic capacitance ,C_d , is defined as:

$$\begin{cases} C_o, & V<V_o,\ \partial V/\partial t>0 \qquad .....(2.16.a) \\ C_o + (C_2 - C_o)f(\eta), & V_o<V<V_2,\ \partial V/\partial t>0 \qquad .....(2.16.b) \\ C_2, & V_2<V<V_m,\ \partial V/\partial t>0 \qquad .....(2.16.c) \\ C_o, & 0<V<V_m,\ \partial V/\partial t<0 \qquad .....(2.16.d) \end{cases}$$

where:

$C_2 = C_2\ (C_0,$ cond.radius),

$f(\eta) = f(V, V_0, V_2, F_1)$,

$V_2 = V_2\ (V_0, V_1, F_1)$,

$V_1 = V_1\ (V_0, p_0,$ cond.radius, front time, $V_m)$,

F_1 = 2 to 3 ,

p_0 = 0.5 to 1.2 .

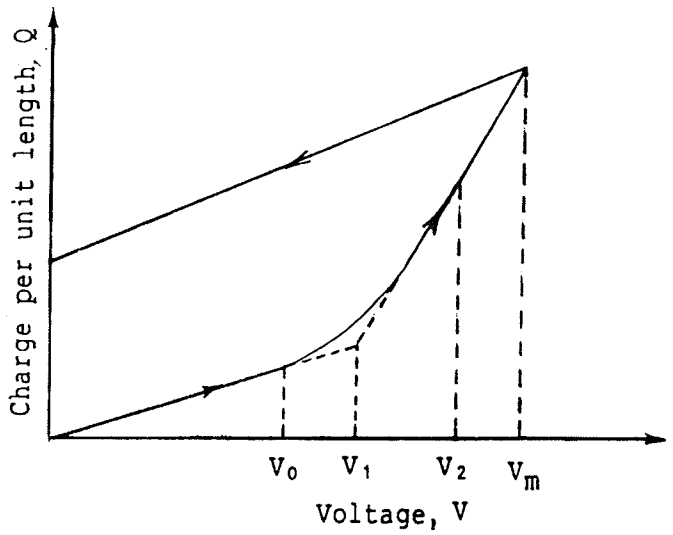

Figure 2.5: A typical Q-V loop used in the approximate Q-V loop model of Gary et.al.

Parameters P_0 and F_1 are chosen to obtain the closest possible agreement between the simplified and experimentally obtained Q-V characteristics for the type of voltage impulses considered by the authors.

The TLE in this model are solved by the Finite Difference Method.

2.1.4 Frequency-Domain Q-V Loop Model

This model has been proposed by N.L. Ovic and G. Kusic.[12] The transient response of a transmission line is obtained in the frequency-domain, and the model includes both the skin and corona effects.

In this model the conductor in corona is assumed to be surrounded by the space charge in the ionization zone, which the authors call "corona cloud". The total charge formed during corona, Q, consists of the charge per unit length bound on the conductor surface, Q_b, and the space charge of the ionization zone, denoted by Q_f, i.e.:

$$Q = Q_b + Q_f \qquad .....(2.17)$$

When the applied voltage is lower than the inception voltage V_0, the capacitance of the line is equal to its geometric capacitance, i.e.

$$C_0 = (2\pi\epsilon_0)/\ln(2h/a) \qquad .....(2.18)$$

where:

h = average suspension height,

a = equivalent radius (GMR) of a conductor bundle

ϵ_0 = permitivity constant .

The geometry used in this model to represent a coronating

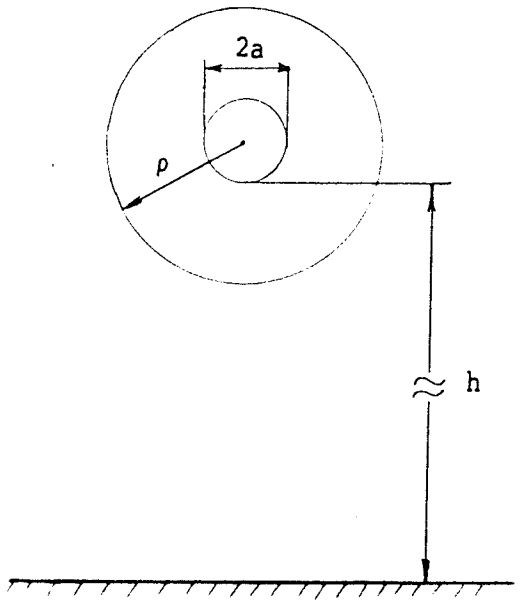

Figure 2.6: Geometry of a coronating conductor used in the frequency-domain Q-V loop model

conductor is shown in Fig.2.6.

Above V_0, the ionization zone is formed and its equivalent radius ρ is defined as the distance from the conductor, where the electric field is equal to the inception value E_0, i.e.:

$$E_0 = Q/(2\pi\rho\epsilon_0) \qquad .....(2.19)$$

By letting $Q=C_0V_0$, the inception voltage, V_0, is obtained as:

$$V_0 = E_0\ a\ \ln(2h/a) \qquad .....(2.20)$$

The electric field within the ionization zone is assumed to be constant and equal to E_0, i.e.

$$E=E_0, \quad a<r<\rho \qquad .....(2.21)$$

and beyond this zone, it has the form:

$$E=Q/(2\pi\rho\epsilon_0), \quad r>\rho \qquad .....(2.22)$$

The applied voltage is equal to the integral of the electric field over the region between the conductor and the ground plane, i.e.

$$V=\int_a^h Edr=\int_a^\rho E_0 dr+\int_\rho^h Edr \qquad .....(2.23)$$

After substituting the charge at the boundary of the ionization zone as $Q=2\pi\rho\epsilon_0 E_0$, the following is obtained:

$$V=E_0(\rho-a)+E_0\rho\ \ln(h/\rho) \qquad .....(2.24)$$

To determine the radius of the ionization zone, ρ, for a given applied voltage, V, this equation is solved iteratively. This is done by rearranging Eq.(2.24) to produce:

$$\rho=(a+V/E_0)/[1+\ln(h/\rho)] \qquad .....(2.25)$$

The calculated radius ρ is used to find the total charge Q, from Eq.(2.22), i.e.:

$$Q=E_0\ 2\pi\rho\epsilon_0 \qquad .....(2.26)$$

For different values of the voltage, different values of Q are obtained. The desired dynamic capacitance is obtained from:

$$C_d = dQ/dV \approx \Delta Q/\Delta V = (Q_n - Q_{n-1})/(V_n - V_{n-1}) \quad \ldots\ldots (2.27)$$

where Q_n, Q_{n-1}, V_n, V_{n-1} are the subsequent values of the total charge Q, obtained by Eq.(2.29), and the applied voltage V, respectively.

Corona losses are modelled independent of the procedure used to model the dynamic capacitance.

Based upon the results of laboratory experiments,[7] the authors developed an approximate Q-V characteristic for each polarity whose shape depends only on the maximum value of the applied voltage impulse. The approximate Q-V characteristics for positive and negative voltage impulses are shown in Fig.2.7. The points d,e,f,r,s, and u on the characteristics are determined graphically by observing the various experimentally recorded Q-V loops and their relationship.

The slope of section a-b on the characteristic in Fig.2.7 is equal to the geometric capacitance of the line. The slope of section b-c is determined by calculation of the dynamic capacitance according to Eq.(2.27). Section c-d has a zero slope and the charge in this section equal to Q , the value which corresponds to the maximum instantaneous value

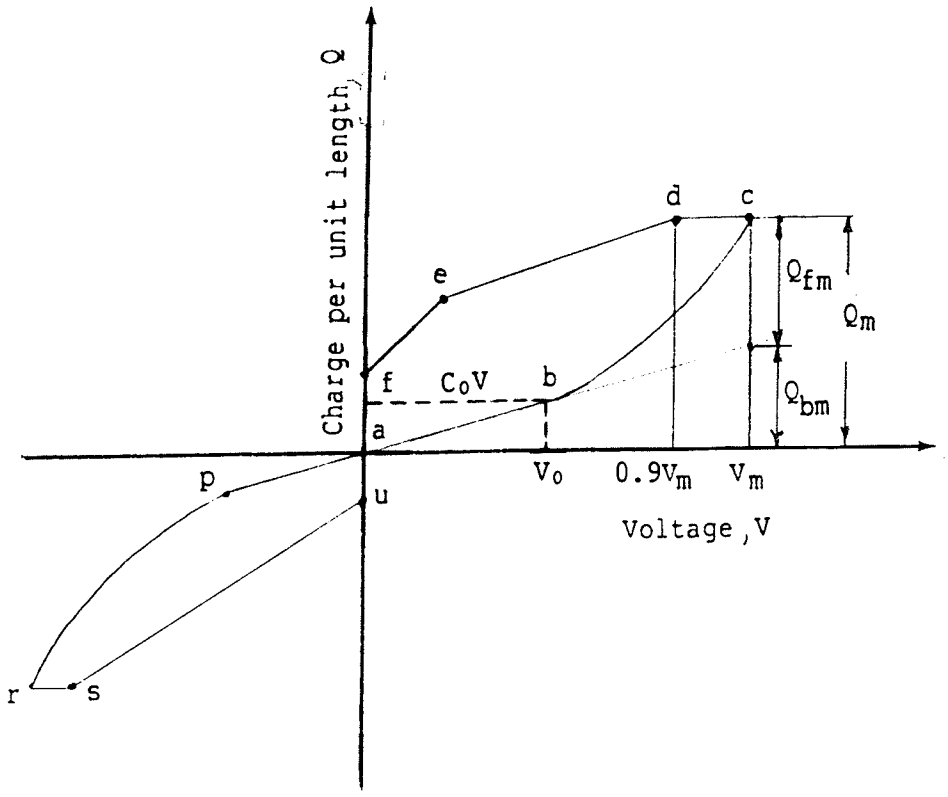

Figure 2.7: Simplified Q-V characteristics used in the frequency-domain Q-V loop model

of the applied voltage. The slope of section d-e is defined as:

$$C_{d-e} = C_o + (1/3)(Q_{fm}/V_m) \qquad \text{.....(2.28)}$$

giving the coordinates of point e as:

$$\text{point e: } [V_o,\ (7/10)(Q_{fm}) + (1/3)(V_o/V_m)Q_{fm} + V_oC_o]$$

The charge Q is identified in Fig.2.7 as the space charge which corresponds to the maximum instantaneous value of the applied voltage. Similarly, the slope of section e-f is defined as:

$$C_{e-f} = C_0 + (1/3)(Q_{fm}/V_m) + (35/200)(Q_{fm}/V_0) \quad ..(2.29)$$

giving the coordinates of point f as:

point f: $(0.0,\ 0.525Q_{fm})$

For negative going waveforms, section a-p-r-s is defined in the same way as for section a-b-c-d. The slope of section s-u is defined as:

$$C_{s-u} = C_0 + (2/3)(Q_{fm}/V_m) \quad .....(2.30)$$

giving the coordinates of point (u) as:

point u: $(0.0,\ -0.4\ Q_{fm})$

The expressions (2.28-2.30) are derived empirically, from the oscillograms recorded in field measurements.[7]

To represent the corona losses in this model,the authors use a resistive element whose value is obtained from

$$W_c = \int I^2\ R_c\ dt \quad .....(2.31)$$

and

$$I = I(t) = V(t)/(Z_0 + R_c) \quad .....(2.32)$$

where Z_0 represents the characteristic impedance of the transmission line defined as:

$$Z_0 = \sqrt{L/C_d} \quad ....(2.33)$$

It should be noted that this impedance is a function of dynamic capacitance C_d defined in Eq.(2.27). Since $Z_0 >> R_c$, Eq.(2.31) becomes:

$$W_c = \int [V(t)/Z_0]^2 \, R_c \, dt \qquad .....(2.34)$$

In the above equation, R_c is assumed to be constant. Hence, it can be removed from the integral and be expressed in the following form:

$$R_c = W_c / \int [V(t)/Z_0]^2 \, dt \qquad .....(2.35)$$

In this equation, the value W_c is determined from the area enclosed by the Q-V loop in Fig.2.7, either for a positive or for a negative voltage pulse.

The resistance R_c is represented as a series resistive

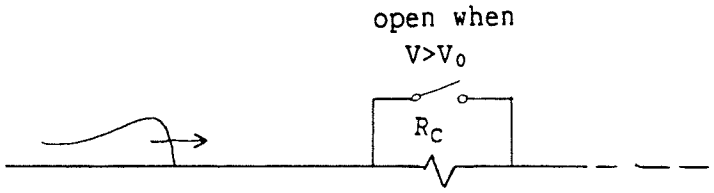

Figure 2.8: Resistive element R_c used in the frequency-domain Q-V loop model to account for corona

element which exists only when $V>V_0$, Fig.2.8.

In order to include the skin effect, the authors use a frequency-dependent longitudinal resistance per unit length which also includes the resistance of the ground return. The solution of the transmission line equations is obtained in frequency-domain by means of the Fourier Series, as described in section 1.4.1.

The authors tested their model in the examples with 2 in., 1.32 in., and 0.927 in. diameter, single-conductor lines subjected to positive and negative lightning voltage impulses whose maximum value ranged from 800 kV to 1750 kV. The lines considered by the authors were assumed to be non-energized.

A weak point of this method is the technique that the authors use to simplify the Q-V characteristics in order to determine the resistive element R_c , i.e. corona losses. This approach could be tolerated if the Q-V characteristics were not dependent on the rate of rise or fall of the voltage pulse. However, this is not true.[13]

Another simplifying assumption used in this model is that the electrical field within the ionization zone is constant and equal to E_0 . In the theory of corona discharges[3], however, it can be found that the electrical field within the ionization zone changes a great deal and may be considered to be equal to E_0 only at the conductor surface.

2.1.5 Approximate Q-V loop model of A.Inoue

This model[14] is based on the time-domain solution of the system of TLE given by Eqs.(1.5) with the resistance and the conductance of the line neglected. An empirically obtained Q-V characteristic, shown in Fig.2.9 is used to obtain the values for the dynamic capacitance, C_d, defined as:

$$\begin{cases} C_0, & V<V_0,\ \partial V/\partial t>0 \quad ..(2.36.a) \\ C_0 + [m_1 k_1 (V-V_0)^{m_1-1}]/V, & V_0<V<V_1,\ \partial V/\partial t>0 \quad ..(2.36.b) \\ C_0 + [m_2 k_2 (V-V_0)^{m_2-1}]/V, & V_1<V<V_m,\ \partial V/\partial t>0 \quad ..(2.36.c) \\ C_0, & 0<V<V_m,\ \partial V/\partial t<0 \quad ..(2.36.d) \end{cases}$$

where:

C_0 = geometrical capacitance of the line [F/m],

V_0 = corona inception voltage [kV],

V_1 = characteristic value of voltage determined experimentally (introduced by the author) [kV],

V_m = maximum value of applied voltage [kV],

k_1, k_2 = constants defined as:

$$k = \sigma_i \sqrt{a/(2h)} \times 10^{-11} \quad [F/m],$$

$i = 1,2$

m_1, m_2 = free parameters [dimensionless],

σ_1, σ_2 = corona loss constants determined empirically [dimensionless],

a = equivalent (GMR) radius of a conductor bundle [m]

h = average suspension height [m].

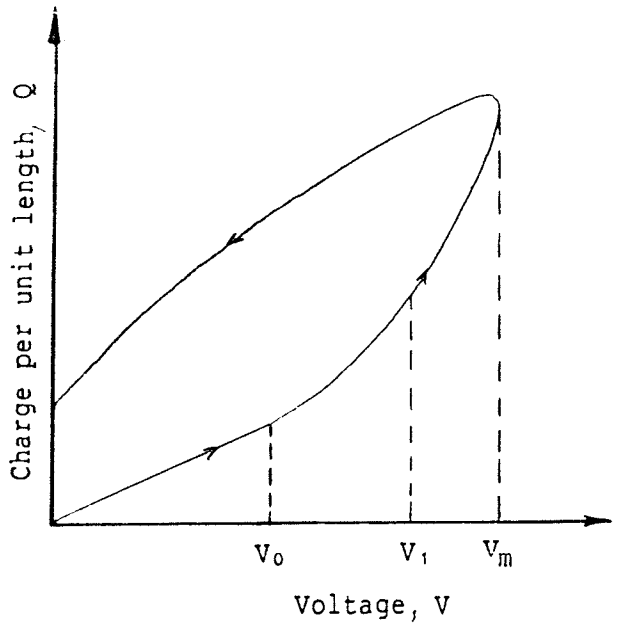

Figure 2.9: A simplified Q-V characteristic used in the approximate Q-V loop model of Inoue

The parameters m_1, m_2, σ_1 and σ_2 as well as V_1 are determined empirically in order to obtain the best possible agreement between the the voltages recorded in field measurements and the results of the numerical simulation with this model. The field measurements were performed on single-conductor, 2-conductor bundle, and four-conductor bundle non-energized transmission lines with 2.24cm and 2.53cm diameter subconductors. The lines were subjected to positive and negative lightning-type voltage impulses whose maximum value ranged from 850 kV to 1720 kV. The values of the model parameters suggested by the author are given in Tabs.2.2 and 2.3.

TABLE 2.2

Geometric and electric line parameters used by Inoue

conductor configur.	h [m]	a [cm]	V_0 [kV]	a_1 [cm]	Z_0 [Ω]
single cond.	22.2	1.265	303	1.265	375
2-cond. bundle	14	1.265	421	1.952	315
4-cond. bundle	14	1.120	599	2.939	250

TABLE 2.3

Values of the empirical constants suggested by Inoue

	V [kV]	V_1 [kV]	σ_1 --	σ_2 --	m_1 --	m_2 --
Impulse 1	1580	1150	30	3	2	2.4
Impulse 2	1130	850	40	15	2	2.2
Impulse 3	850	700	45	20	2	2.2

The TLE are solved by the Finite Difference Method using a time step of $\Delta t=0.01$ μs and a displacement step of $\Delta x=7.05$ m.

In Tab.2.2, a_1 is defined by the author as the radius of an equivalent single conductor whose maximum surface field strength is equal to that of the bundled conductor. The characteristic impedance of the line ,Z_0, is obtained by measurement at a voltage below V_0 . Also, the values for C_0 are calculated from the value of Z_0 and the conditions of surge propagation at the speed of light.

TABLE 2.2

Geometric and electric line parameters used by Inoue

conductor configur.	h [m]	a [cm]	V_0 [kV]	a_1 [cm]	Z_0 [Ω]
single cond.	22.2	1.265	303	1.265	375
2-cond. bundle	14	1.265	421	1.952	315
4-cond. bundle	14	1.120	599	2.939	250

TABLE 2.3

Values of the empirical constants suggested by Inoue

	V [kV]	V_1 [kV]	σ_1 --	σ_2 --	m_1 --	m_2 --
Impulse 1	1580	1150	30	3	2	2.4
Impulse 2	1130	850	40	15	2	2.2
Impulse 3	850	700	45	20	2	2.2

The TLE are solved by the Finite Difference Method using a time step of $\Delta t=0.01$ μs and a displacement step of $\Delta x=7.05$ m.

In Tab.2.2, a_1 is defined by the author as the radius of an equivalent single conductor whose maximum surface field strength is equal to that of the bundled conductor. The characteristic impedance of the line ,Z_0, is obtained by measurement at a voltage below V_0 . Also, the values for C_0 are calculated from the value of Z_0 and the conditions of surge propagation at the speed of light.

TABLE 2.4

Key features of the reviewed models

	Single Shell Model[9]	Conductance Model[10]	Frequency Domain Q-V Loop Model[12]	Q-V Loop Model[14]	Approximate Q-V Loop Model[11]
Authors	Harrington, Afghani	Lee	Ovic, Kusic	Inoue	Gary, Timotin, Cristescu
solution technique	time-domain using modal transformation	solve the TLE in time-domain by FDM	solve the TLE in frequency-domain by Fourier Series	solve the TLE in time-domain by FDM	solve the TLE in time-domain by FDM
type of Q-V characteristics	approximate Q-V loops	single-valued Q-V charact.	approximate Q-V loops	approximate Q-V loops	approximate Q-V loops
technique used to obtain the Q-V characteristics	numerically generated by the model	empirically by comparison of computed and experimentally recorded waveforms	empirically by graphical approximation of experimentally recorded Q-V loops	empirically from experimentally recorded Q-V loops	empirically from experimentally recorded Q-V loops
corona losses modelling technique	by means of current sources between the line and the ground	by means of nonlinear voltage dependent conductance G determined from Peek's Law for corona losses	by means of a series resistance R_C determined from the area enclosed by the approximate Q-V loop	already included by the approximate Q-V loop	already included by the approximate Q-V loop

TABLE 2.5

Key features of the examples used for numerical simulation with the reviewed models

	Single Shell Model[9]	Conductance Model[10]	Frequency Domain Q-V Loop Model[12]	Q-V Loop Model[14]	Approximate Q-V Loop Model[11]
Authors	Harrington, Afghani	Lee	Ovic, Kusic	Inoue	Gary, Timotin, Cristescu
impulse polarity	+	+,-	+,-	+,-	+
conductor-bundle configuration/V_o	1x30.5 mm/219 kV 4x30.5 mm/490 kV 1x20.5 mm/350 kV 1x23.5 mm/220 kV	1x25.3 mm/277 kV 4x22.4 mm/588 kV	1x51.0 mm/400 kV 1x23.6 mm/220 kV 1x13.2 mm/150 kV	1x25.3 mm/303 kV 1x23.3 mm/421 kV 4x22.4 mm/599 kV	1x26.4 mm/320 kV
max. amplitude of the applied impulses [kV]	390 to 610	1500	800 to 1550	850 to 1720	1050 to 1120
types of applied voltage impulses	lightning, switching	lightning	lightning	lightning	lightning
max. voltage rate of rise [kV/μs]	66.6	1000	2150	2188	5600
min. voltage rate of rise [kV/μs]	8.8	750	1317	400	933

2.2 Finite Difference Representation of TLE

The Finite Difference Method (FDM) is frequently used as a method for solving the system of TLE in the time-domain. Its simplicity is the main reason that this method was chosen for the overvoltage propagation analyses in the remaining sections of this and the next chapter. Before proceeding with an analysis using this method, a detailed description of the method, as well as its limitations, will be presented.

Generally, the finite difference representations of the first derivative of any differentiable two-argument function F(x,t) are:

$$\partial F/\partial x=[F(x+1,t)-F(x,t)]/\Delta x \qquad .....(2.37)$$

$$\partial F/\partial t=[F(x,t+1)-F(x,t)/\Delta t \qquad .....(2.38)$$

In the theory of finite differences, these expressions are known as forward differences. Using these forms for the derivatives in Eqs.(1.5), the finite difference representation of the TLE is:

$$-[I(x+1,t)-I(x,t)]/\Delta x=C_d\ [V(x,t+1)-V(x,t)]/\Delta t + G\ V(x,t) \qquad .....(2.39a)$$

$$-[V(x,t+1)-V(x-1,t+1)]/\Delta x=L_0\ [I(x,t+1)-I(x,t)]/\Delta t + R_0\ I(x,t) \qquad .....(2.39b)$$

After rearranging, these equations become:

$$V(x,t+1)=AV(x,t)-B[I(x+1,t)-I(x,t)] \qquad .....(2.40a)$$

$$I(x,t+1)=CI(x,t)-D[V(x,t+1)-V(x-1,t+1)] \qquad ...(2.40b)$$

where:

$$A = 1-\Delta t/(G\ C_d) \qquad \ldots\ldots(2.41.a)$$

$$B = \Delta t/(C_d\ \Delta x) \qquad \ldots\ldots(2.41.b)$$

$$C = 1-\Delta t(\ R_o/L_o\ ) \qquad \ldots\ldots(2.41.c)$$

$$D = \Delta t/(\ L_o\Delta x\ ) \qquad \ldots\ldots(2.41.d)$$

The computation is started at $x=\Delta x$ and $t=\Delta t$ using equation (2.40.a) with the following boundary and initial conditions:

$$V(x,0)=V_{SS} \qquad V(0,t)=E(t)$$

$$I(x,0)=0$$

where E(t) represents the input pulse and V a value of the steady-state voltage.. Equation (2.40.b) is then used to compute the new current values I(x,t+1) using the new values of the voltages V(x,t+1) and V(x-1,t+1). During each time step, the values of the voltages and the currents are computed all along the line according to an appropriately chosen displacement step Δx.

According to the theory of finite differences,[4] for the numerical procedure to be stable, the following condition (Courant-Friedrich-Lewy) must be satisfied:

$$(\Delta t/\Delta x)/(\ \sqrt{L_oC_o}\ ) \leq 1$$

This is the condition of stability for the finite difference approximation of the hyperbolic partial differential equation. The condition can be satisfied by adjusting the ratio $\Delta t/\Delta x$.

3. COMPARISONS

Three models have been chosen for comparison from those that were reviewed in section 2.1. All three models are applicable for the analyses of transient phenomena on HVDC transmission lines. In order to obtain a valid comparison, they are all analyzed using the Finite Difference Method (FDM).

3.1 Application of the Finite Difference Method (FDM)

Before comparing the different models using the FDM, it is necessary to investigate the accuracy obtained by the implementation of FDM.

As a test example, a lossless transmission line with the parameters C_0 = 8.89 nF/km and L_0 = 1.25 mH/km was chosen. The propagation of a 1200 kV, 1.2/50 μs standard lightning impulse along the line energized with zero steady-state voltage was simulated. The results of the simulation were compared with the analytical solution for this case. The error was expressed in the form of standard deviation defined as;

$$\sigma = \sqrt{\sum_{i=1}^{N} [V(x,i) - V_b(x,i)]^2 / N} \qquad \ldots\ldots(3.1)$$

where:

$V(x,i)$ = value of the calculated voltage at distance x and at time $t=i\,\Delta t$,

$V_b(x,i)$ = base value for voltage at the same time and location as $V(x,i)$ (from the analytical solution or from experiments)

N = number of discrete values of voltages (N=1000)

The standard deviation given in Tab.3.1 was calculated in the following three time ranges:

Time Range A (range of the front): 0.0-1.3 μs

Time Range B (range of the crest): 1.3-3.0 μs

Time Range C (range of the tail): 3.0-6.0 μs

The choice of a time step of $\Delta t=0.01$ μs and a displacement step of $\Delta x=6$ m used for these calculations resulted in a stability factor of 0.50 .

Using the same time step, the problem was simulated with the Electromagnetic Transient Program (EMTP). The numerical results were obtained at the same distances as before and compared with the analytical solution. Again, the error had a form of the standard deviation calculated within the same three ranges. These results are also shown in Tab.3.1

It can be noted that the EMTP consistently gives slightly more accurate results. However, this difference

TABLE 3.1

Comparison of the performances of EMTP and FDM in terms of the standard deviation for a lossless line subjected to a 1200 kV, 1.2/50 μs voltage impulse

STANDARD DEVIATION [kV] - FDM			
	X=360m	X=720m	X=1080m
Time Range A	0.7384	0.6054	0.7299
Time Range B	0.3091	0.4794	0.6541
Time Range C	0.2396	0.4123	0.5914
STANDARD DEVIATION [kV] - EMTP			
Time Range A	0.5138	0.3675	0.5965
Time Range B	0.1841	0.3927	0.5808
Time Range C	0.1922	0.3758	0.5546

was found to be negligible for the simulations performed in this work and, therefore, the FDM is chosen for modelling purposes in the present study.

3.2 Comparison of Corona Models

Among the models reviewed in section 2.1, the conductance model,[10] the approximate Q-V loop model of Gary et al[11], and the Q-V loop model of Inoue[14] were chosen for comparison.

There are several reasons to account for this choice. First, all three models are time-domain based models and represent the typical modeling techniques used in this domain. Second, the other two reviewed models, are based on some assumptions which would greatly limit their application

in HVDC transmission systems (sections 2.1.1 and 2.1.4). Besides, one of them is a frequency-domain based model which was found to be inconvenient for this study.

The model of Gary et al, in addition to corona effect, also includes the skin effect, whereas the other two models deal with the corona effect only. In order to obtain valid comparisons of these three models, from the point of view of modelling the corona effect, this model was modified by excluding the skin effect. This was achieved by setting the line resistance in the model to zero. This modification does not affect the analysis of the influence that corona has on overvoltage travelling waves, because there is no interaction between these two phenomena.

The comparison was carried out using the same transmission line geometry as that considered by both Lee[10] and Inoue[14], which is:

a) line inductance, L_0 1.25 mH/km
b) geometric line capacitance, C_0 8.89 nF/km
c) equivalent radius of conductor,a 12.65 mm
d) average suspension height,h 22.20 m.
e) number of conductors in a bundle, 1
f) steady-state voltage of the line, V 0. kV

The input waveform used by Lee is shown in Fig.3.1 and that used by Inoue in Fig.3.5. These input waveforms were recorded, experimentally, on the transmission line of the

geometry described as above. It can be noted that although the line geometry was the same, the values of the inception voltage were different. This can only be explained as a result of using different expressions for calculating the inception voltage. Unfortunately, the authors did not provide sufficient information about calculating V_0 .

The purpose of the comparison carried out in this section was to verify the results published by Lee and Inoue and compare those results with the results obtained by using different modelling techniques. The comparison of the models was carried out choosing infinitesimal segments of distance and time as Δx=7.05 m and Δt=0.01 μs, respectively. These values resulted in a stability factor of 0.425

The values of the parameters in the conductance model are listed in Tab.2.1. For the purpose of the comparison study in this section, the model parameters had values that correspond to a single-conductor transmission line configuration and a positive voltage impulses.

The values of parameters used in the Q-V loop model of Inoue are listed in Tabs.2.2 and 2.3. The comparison study in this section was carried out with the values that correspond to a single-conductor configuration, and the voltage impulse denoted by 2, Tab.2.3.

The set of adjustable parameters in the modified Q-V loop model of Gary et al consists of parameters F_1 and p_0 . It was found that the best agreement between numerical and

the experimental results were obtained with the following values of these parameters:

$$F_1 = 2.3$$

$$p_o = 0.8$$

First, the waveform shown in Fig.3.1 was used as the input waveform for each of the three compared models. For each model, the voltages were computed at the distances of 352.5m, 705m, and 1057.5m. These results were compared with the experimental results recorded by Lee at the same distances. The results from the models were assessed by comparing the standard deviation computed according to Eq.(3.1) where the base value at any location on the line was the experimentally recorded value by Lee[10] at that location The standard deviations given in Tab.3.2 were calculated for the following three time ranges:

1. Time Range A (range of the front) 0-2 μs
2. Time Range B (range of the crest) 2-3 μs
3. Time Range C (range of the tail) 3-4 μs

The experimental and computed voltage waveforms are shown in Figs.3.2-3.4.

The same kind of comparison was carried out using the waveform shown in Fig.3.5 as the input waveform for each of the three models. The voltages were computed at the same distances and using the same time and displacement steps as before. These results were compared with the experimental results recorded by Inoue. The errors are calculated for each of the three models using the same technique as in the previous case, and the results are shown in Tab.3.3. The experimental and computed voltage waveforms are illustrated in Figs.3.6-3.8.

TABLE 3.2

Comparison in terms of the standard deviation between voltages computed by different models and voltages experimentally obtained by Lee

STANDARD DEVIATION [kV]

Conductance Model[10] - Lee			
	X=352.5m	X=705m	X=1057.5m
Time Range A	52.75	59.29	80.82
Time Range B	36.72	24.42	87.38
Time Range C	73.27	101.71	246.80
Q-V loop model[14] - Inoue			
Time Range A	64.12	73.30	78.60
Time Range B	57.67	111.03	43.94
Time Range C	50.28	60.71	258.52
Approximate Q-V loop model[11] - Gary			
Time Range A	105.87	118.26	126.13
Time Range B	112.45	210.87	335.18
Time Range C	25.10	81.87	469.56

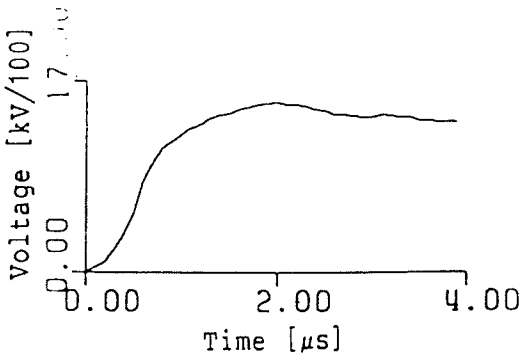

V_0 = 277 kV

Figure 3.1: Input waveform used by Lee

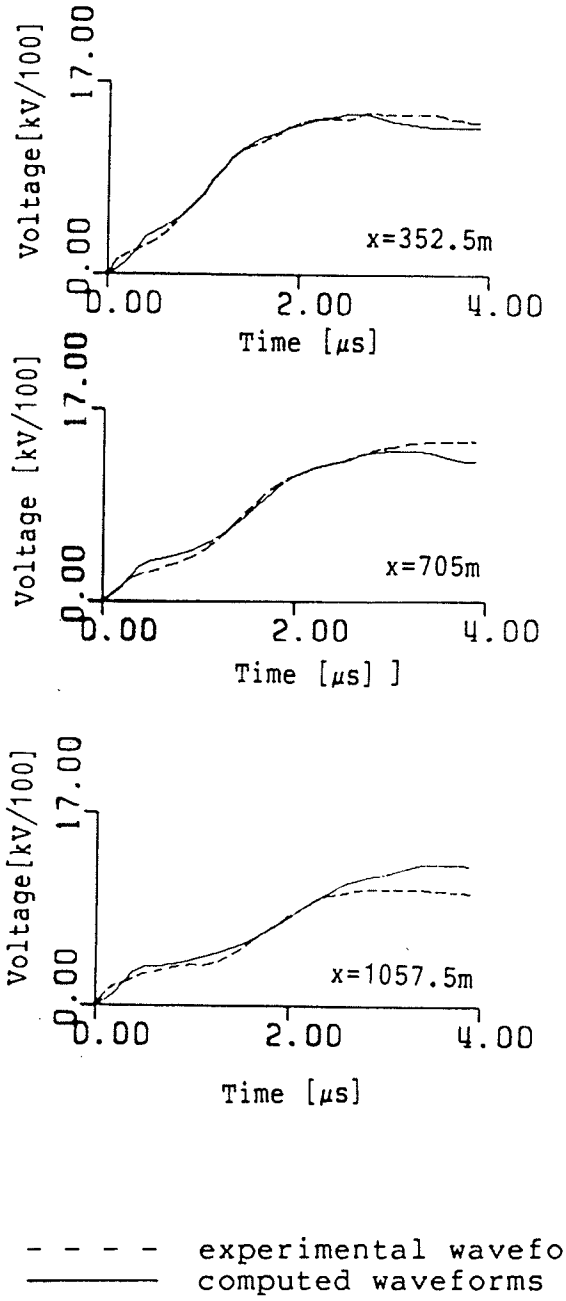

Figure 3.2: Comparison between waveforms computed by the conductance model[10] and experimental waveforms obtained by Lee

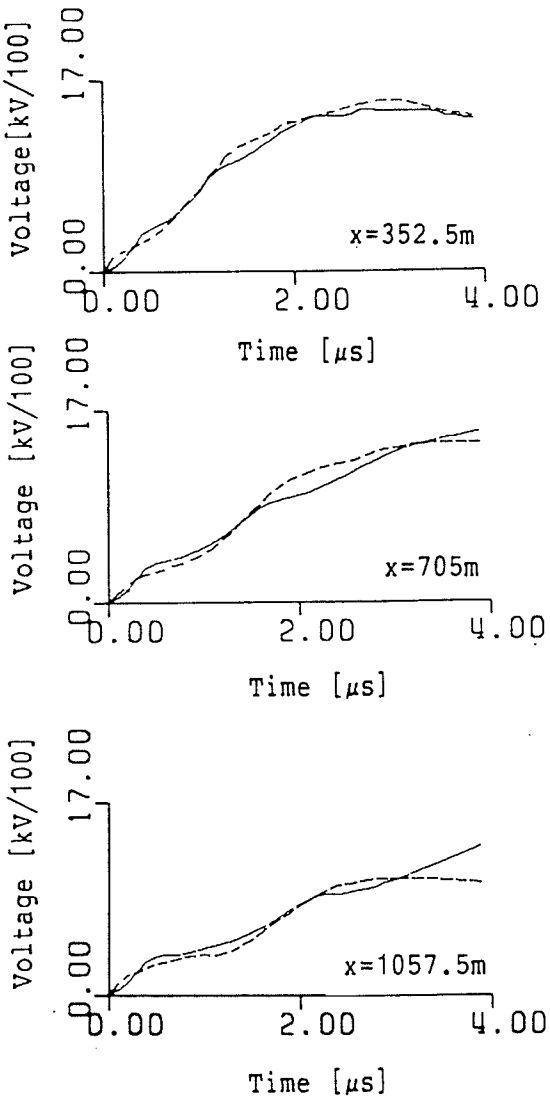

Figure 3.3: Comparison between waveforms computed by the Q-V loop model[14] and experimental waveforms obtained by Lee

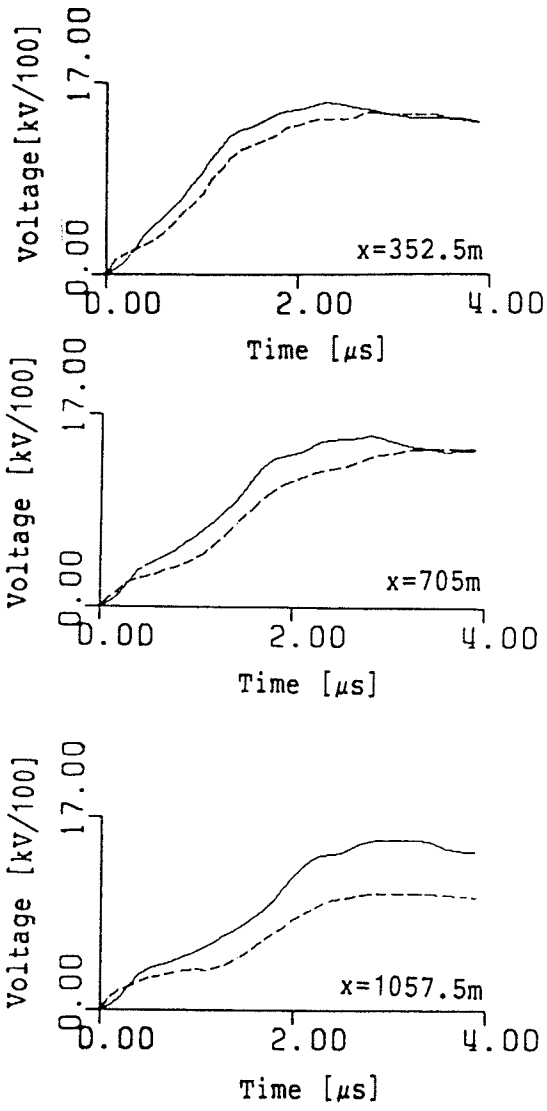

- - - - experimental waveforms
------- computed waveforms

Figure 3.4: Comparison between waveforms computed by the approximate Q-V loop model[11] and experimental waveforms obtained by Lee

TABLE 3.3

Comparison in terms of the standard deviation between voltages computed with different models and voltages experimentally obtained by Inoue

STANDARD DEVIATION [kV]

	X=352.5m	X=705m	X=1057.5m
Conductance model[10] - Lee			
Time Range A	67.55	69.40	68.29
Time Range B	46.46	76.14	54.50
Time Range C	44.32	65.24	95.98
Q-V loop model[14] - Inoue			
Time Range A	116.28	70.99	116.39
Time Range B	50.87	112.53	129.53
Time Range C	59.79	11.640	141.49
Approximate Q-V loop model[11] - Gary			
Time Range A	98.26	185.51	159.24
Time Range B	65.74	303.56	386.99
Time Range C	62.05	140.32	387.76

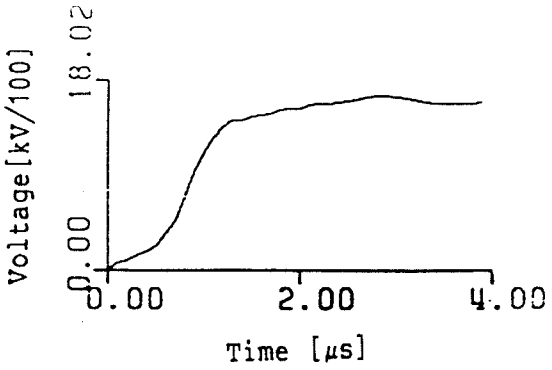

V_0 = 301 kV

Figure 3.5: Input waveform used by Inoue

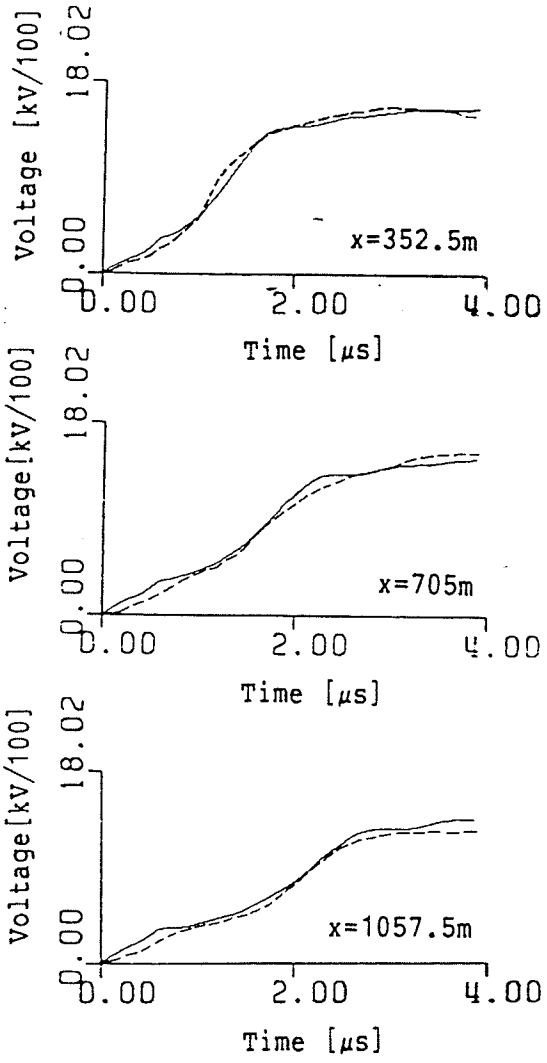

- - - - experimental waveforms
------- computed waveforms

Figure 3.6: Comparison between waveforms computed by the conductance model[10] and experimental waveforms obtained by Inoue

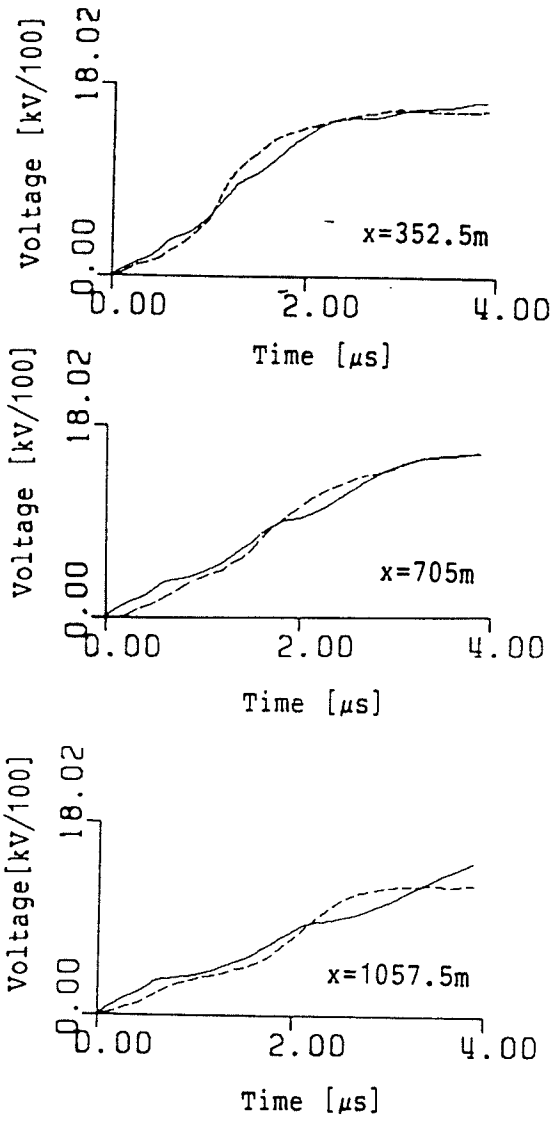

- - - - experimental waveforms
------- computed waveforms

Figure 3.7: Comparison between waveforms computed by the Q-V loop model[14] and experimental waveforms obtained by Inoue

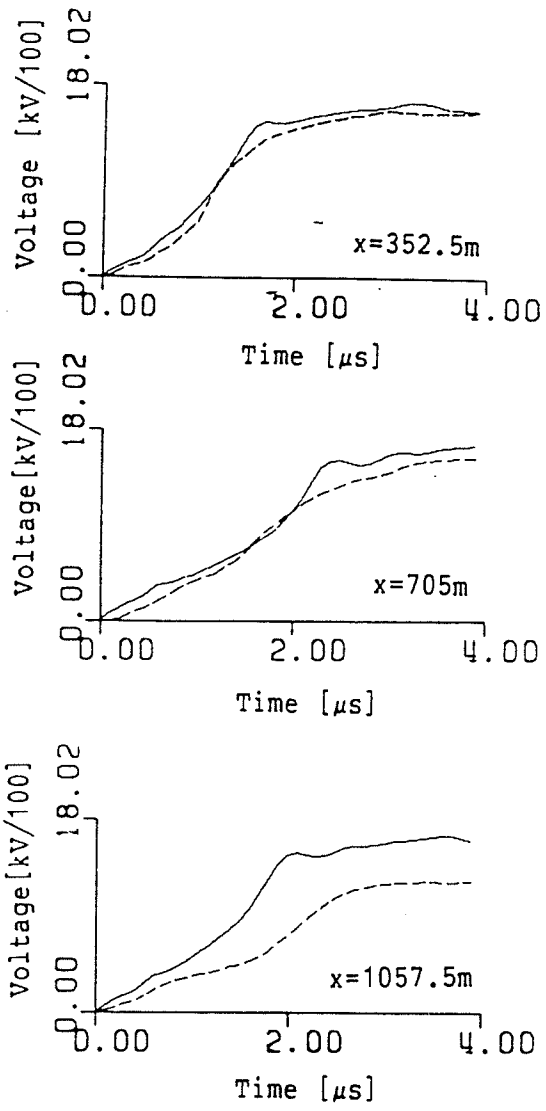

- - - - experimental waveforms
------- computed waveforms

Figure 3.8: Comparison between waveforms computed by the approximate Q-V loop model[11] and experimental waveforms obtained by Inoue

3.3 Conclusion

Comparison of the models in section 3.2 was carried out through numerical simulation of transient conditions on a single-conductor transmission line. The simulation was done using two different, experimentally derived, lightning-type input waveforms. The results of this comparison, shown in Figs.3.2-3.4 and 3.6-3.8 and in Tabs.3.2 and 3.3, indicated that the model with highest accuracy is the conductance model. Slightly less accurate results were obtained with the Q-V loop model of Inoue and much less accurate ones with the approximate Q-V loop model of Gary et al. The less accurate performance of the Q-V loop models under consideration can only be explained by inaccurate modelling of the experimental Q-V characteristics.

It can be noted that each of the compared models is based on a different number of empirically determined constants. These constants describe the increase of capacitance and/or conductance beyond the corona inception voltage and depend on conductor bundle configuration as well as the shape and polarity of voltage impulses. They have to be determined through an optimization process which implies the availability of experimental results. The degree of difficulty in deriving the appropriate values of these constants determines the practical applicability of these models. The conductance model, which turned out to be the most accurate of the compared models, is based on two

empirical constants, whereas the slightly less accurate Q-V loop model of Inoue is based on five empirical constants. Since it is much easier to optimize a model with two, than a model with five adjustable constants, it is evident that the conductance model has a higher practical applicability. Therefore, considering both the accuracy and practical applicability of the models, it is suggested that the conductance model should be utilized for modelling corona on HVDC transmission lines.

4. CORONA MODEL IMPLEMENTATION ON HVDC TRANSMISSION LINES

The results presented in Chapter 3 indicate that from the point of view of accuracy and practical application, the conductance model[10] is the most suitable of the reviewed models for implementation in an HVDC transmission system. Since overvoltage transients usually occur when an HVDC line is energized, a few additional assumptions must be included in this model to accommodate this condition.

4.1 Important Assumptions

Normally, the steady-state operating voltage of HVDC transmission lines is approximately 30% higher than the corona inception voltage. This implies that an HVDC line already coronates under steady-state conditions. If the line is subjected to an overvoltage surge, the intensity of ionization changes and it is accommodated through a change of voltage-dependent transmission line parameters. In order to analyze the performance of an HVDC transmission line under these conditions, the following assumptions were made:

1. Voltage-dependent steady-state transmission line parameters are determined by the intensity of corona under steady-state conditions. Since the

steady-state voltage is always higher than the corona inception voltage, the parameters are determined according to Eqs.(2.13) and (2.14).

2. If an energized line is subjected to an overvoltage surge of polarity opposite to that of the energized line, and of an amplitude which is higher than 2.0 p.u., impulse corona is considered to start when the absolute value of the steady-state voltage is exceeded. As long as this value is not exceeded, the voltage-dependent line parameters are assumed to be constant and to have the values that correspond to the steady-state conditions.
3. In the case when the surge is chopped either on the front or on the tail, the transmission line parameters are assumed to be constant and to have the values determined by the maximum value of the applied voltage after this value of the voltage is reached.

Assumption 2 may yield attenuation values that are slightly higher than that which can occur in reality. Assumption 3 affects the tail of a computed waveform, resulting in attenuation that is slightly higher than that which can normally occur. The peak value, however, is not affected by this assumption at all.

4.2 Parameters of the Model

The adopted corona model has 2 sets of parameters. One set of parameters depends solely on the transmission line geometry and is comprised of:

R = line resistance per unit length,

L_0 = line inductance per unit length,

C_0 = geometric capacitance of the line per unit length,

V_0 = corona inception voltage.

The other set consists of the dynamic capacitance, C_d, and the conductance, G, which depend on both the geometry and the applied voltage, and therefore, are affected by corona.

The influence of the steady-state resistance, R, was found to be negligible. Since the skin effect is neglected in the present study, a resistance of zero is assumed.

4.2.1 Transmission Line Inductance, L_0

The line inductance, L_0, is represented as a sum of the external component, L_e, and the internal component, L_i, i.e.

$$L_0 = L_e + L_i \qquad .....(4.1)$$

where:

$$L_e = (\mu_0 / 2\pi)\ln(2h/a) \qquad ..... (4.1.a)$$

$$L_i = \mu_0 / 8\pi \qquad ..... (4.1.b)$$

h = average suspension height,

a = equivalent radius (GMR) of a conductor bundle,

μ_0 = permeability of air ($\mu_0 \approx 4\pi x10^{-7}$ H/m).

The equivalent radius of bundled conductors is determined as the Geometric Mean Radius of a bundle (GMR).

4.2.2 Geometric Capacitance of the Line, C_0

The capacitance, C_0, is determined from the following expression:

$$C_0 = (2\pi\epsilon_0)/\ln(2h/a) \qquad .....(4.2)$$

where:

ϵ_0 = permitivity of the air ($\epsilon_0 \approx 8.85 \times 10^{-12}$ F/m)

This capacitance is the line capacitance under non-corona conditions.

4.2.3 Corona Inception Voltage, V_0

Corona inception voltage is determined from the expression proposed by C.F. Wagner[2] which can be used for monopolar HVDC transmission lines, i.e.:

$$E_0 = [2V_0 (1+B)]/[n\ d\ \ln(2h/a)] \qquad .....(4.3)$$

where:

E_0 = inception voltage gradient [kV/cm],

V_0 = corona inception voltage [kV],

n = number of subconductors in a bundle [dimensionless],

d = diameter of the subconductors [cm],

a = equivalent radius (GMR) of a conductor bundle [cm],

h = average suspension height [cm],

B = bundling coefficient:

B = B(d,s) [dimensionless],

s = spacing between subconductors [cm].

The coefficient, B, is introduced to account for the influence of the charges on other subconductors. The expressions that define this coefficient for different

TABLE 4.1

Values of the bundling coefficient B^2

n	1	2	3	4	6
B	0	d/s	3.64d/2s	4.24d/2s	5.31d/2s

bundle configurations are given in Tab.4.1. Corona inception voltage, V_0, is obtained from Eq.(4.3) as:

$$V_0 = E_0\, n\, d\, \ln(2h/a)/[2(1+B)] \qquad .....(4.4)$$

The values for the corona inception voltage gradient, E_0, are determined from Peek's equation[2], i.e.:

$$E_0 = 30m[1+(0.301/\sqrt{a})] \quad [kV/cm] \qquad .....(4.5)$$

where:

m = conductor surface factor [dimensionless],

a = equivalent radius (GMR) of a conductor bundle [cm].

The value of the factor m depends on the type of conductor and the weather conditions. For the 4.06 cm diameter conductor used for the Nelson River line, the values for m are accepted to be 0.5 for summer, and 0.6 for winter.[2] According to the experimental results,[8] the values for E_0 determined by Eq.(4.5) are in agreement with measured values for switching impulses. For lightning impulses however, it has been indicated[8] that this value should be increased by about 10 to 15%.

3.2.4 Dynamic Capacitance, C_d

The dynamic capacitance is fully defined by Eqs.(2.13). It can be noted that this parameter is a function of the applied voltage, the line geometry and a corona loss constant which is determined empirically, i.e.:

$$C_d = C_d(V, V_0, a, h, \sigma_1) \qquad \ldots\ldots(4.6)$$

where:

V = instantaneous value of the applied voltage [kV],

V_0= corona inception voltage [kV],

a = equivalent radius (GMR) of a conductor bundle [m],

h = average suspension height [m],

σ_1 = empirical corona loss constant [dimensionless].

The corona loss constant σ_1 determines the rate of increase of the dynamic capacitance beyond the geometric value. Experimental results[8] indicate that the value of σ_1:

- is larger for impulses of positive polarity
- is larger under fair weather conditions
- increases with the steepness of an impulse
- increases with the conductor diameter
- decreases as the number of conductors in a bundle increases

This constant can only be determined empirically, by comparison of computed and measured voltages at a position on the line. For example, for a monopolar line with the same conductor configuration as that used for the Nelson River line, σ_1 is determined to be 30 for positive voltage impulses of the lightning-type.[10]

Fig 4.1 shows the variation of the dynamic capacitance, as a function of the applied voltage, when the same line, in a non-energized condition, is subjected to a 900 kV, 1.2/50 μs positive voltage impulse.

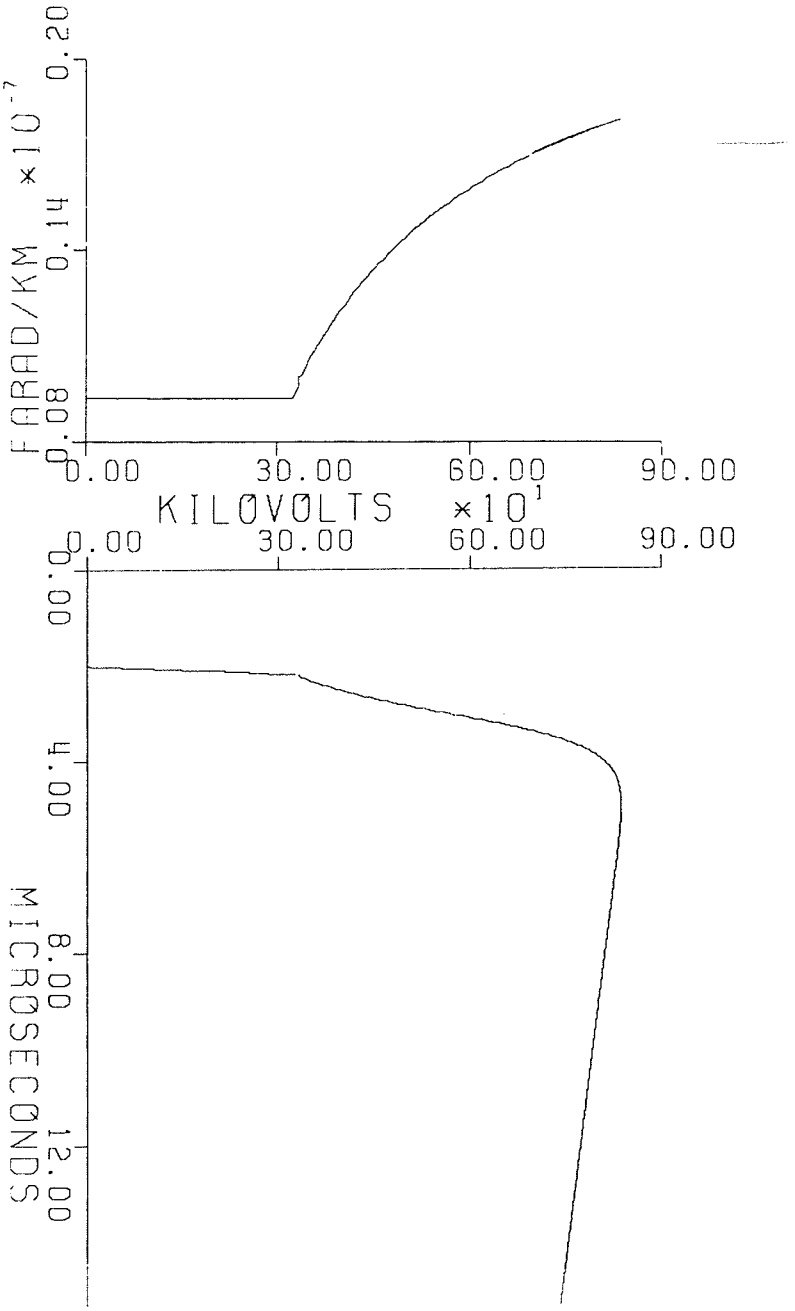

Figure 4.1: Dynamic capacitance v.s. applied voltage for the Nelson River conductor bundle configuration. Fair weather conditions. Positive voltage impulse. Non-energized line.

3.2.5 Transmission Line Conductance, G

When a transmission line is not in corona, the conductance of the line, G, is very small and it is usually neglected. In the case of a coronating transmission line, this parameter is fully defined by Eq.(2.14). Using the same notation as that used to describe C_d, the conductance, G, can be represented as:

$$G = G(V, V_0, a, h, \sigma_2) \qquad .....(4.7)$$

where V, V_0, and h have the same significance as in Eq.(4.6). The constant σ_2 is another empirical corona loss constant which depends on the intensity of energy dissipation for a conductor in corona. It is obtained through a comparison analysis similar to that used to obtain σ_1. This constant affects the attenuation of a voltage impulse, whereas its influence on the steepness of a voltage impulse is negligible. According to experimental results,[8] this constant depends on:

- weather conditions
- conductor bundle configuration
- polarity of a voltage impulse
- duration of a voltage impulse

For a specific weather condition and impulse polarity, the energy dissipated by corona has been shown[8] to depend mainly on the total duration of the voltage impulse, rather than on the steepness of its front.

For example, according to experimental results,[10] this constant is determined to be $1x10^7$ for the monopolar line under consideration, positive voltage impulses of the lightning-type, and a fair weather condition. The variation of the line conductance as a function of the applied voltage when the non-energized line was subjected to 900 kV, 1.2/50 μs positive voltage impulse is shown in Fig.4.2.

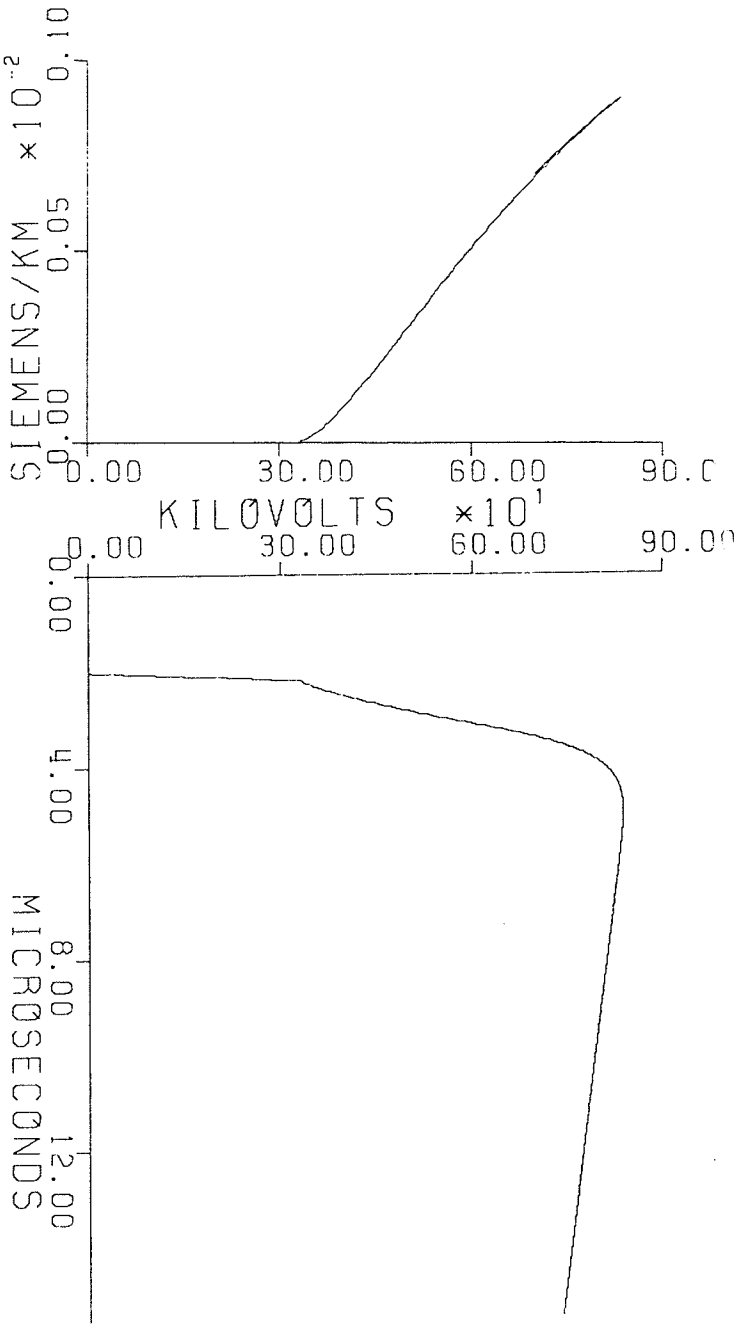

Figure 4.2: Conductance v.s. applied voltage for the Nelson River conductor bundle configuration. Fair weather condition. Positive voltage impulse. Non-energized line.

4.3 Parameters of the Line Used for Simulation

For the numerical simulations, a two-conductor bundle monopolar HVDC semi-infinite transmission line was considered. The configuration of the bundle is the same as that used for the Nelson River transmission line. The geometry of the line is shown in Fig.4.3 and the parameters

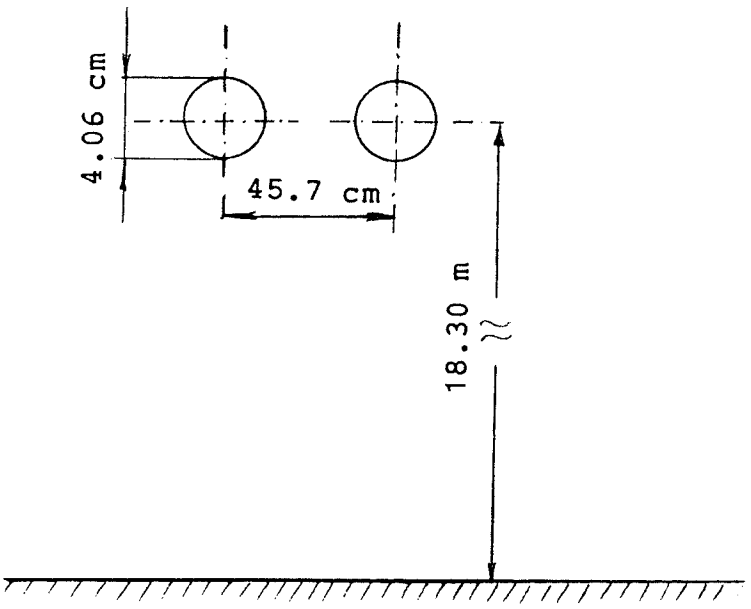

Figure 4.3: Nelson River conductor bundle geometry

of the line are given in Tab.4.2.

The corona inception voltage gradient, E_0, was calculated according to Eq.(4.5), using a value of 0.5 for the conductor surface factor, m, and assuming a single-conductor configuration of the bundle. This assumption is justified by the fact that the bundling effect on the inception

TABLE 4.2

Electrical parameters of a monopolar HVDC transmission line with the Nelson River conductor bundle configuration

Parameter		Symbol	Value
Steady-state operating voltage		V_{SS}	+450 kV 0 -450 kV
Line inductance		L_0	1.238 mH/km
Geometric capacitance		C_0	9.360 nF/km
Corona inception voltage gradient (Peek)	Lightning impulse	E_0	20.89 kV/cm
	Switching impulse		18.17 kV/cm
Corona inception voltage (Wagner)	Lightning impulse	V_0	318 kV
	Switching impulse		277 kV

voltage is negligible when the spacing between the subconductors is large. The spacing between them can be considered as large if the ratio between the spacing and the subconductor diameter is greater than 10. In other words, corona starts independently on both subconductors as in a single-conductor arrangement. For the same reason, the empirical corona loss constants in the model, σ_1 and σ_2, have the same values as for a single-conductor configuration, Tab.4.3. These values are obtained for positive voltage impulses and a fair weather condition.

The values for lightning impulses are those determined by Lee,[10] and can be used only for this kind of voltage impulses. For switching-type voltage impulses, however, the values of σ_1 and σ_2 are estimated from experimental results[8] obtained for a line with a conductor bundle configuration similar to that of the Nelson River line. The new values are estimated by means of a Q-V loop recorded for a 1.82 in. conductor and a fair weather condition, when a switching-type voltage impulse is applied at the beginning of the test line. The value of σ_1 is obtained by adjusting its value in the expression for C_d, Eq.(2.13.b.), in order to obtain the calculated value of C_d equal to that determined from the slope on the Q-V loop at the point that corresponds to the same applied voltage above the inception value. Similarly, the value of σ_2 is obtained through the process of adjusting its value in the expression for G, Eq.(2.14), in order to obtain the same energy dissipated by corona as that determined from the area enclosed by the Q-V loop.

TABLE 4.3

Values of empirical corona loss constants σ_1 and σ_2 for positive voltage impulses, a fair weather condition and the Nelson River conductor bundle configuration

waveform type	σ_1	σ_2
lightning	30	1×10^7
switching	12	1.09×10^5

4.4 Description of the Waveforms Used for Simulation

The numerical simulation was carried out using the input voltage waveforms in the form of positive 1.2/50 μs standard lightning, and 250/2500 μs standard switching voltage impulses. Since practical experience with the Nelson River line indicates that the line voltage under transient conditions seldom exceeds 2.0 p.u., the amplitude of these impulses was chosen as 450 kV. Under such circumstances, the situation when the polarities of the steady state voltage and the voltage impulse are opposite has no practical significance and, therefore, was not simulated. The simulation was carried out with full and chopped standard lightning waveforms; the waveforms were chopped at either the front or the tail.

The full waveforms are generated by the following double exponential form:

$$E(t) = E_1 \left[\exp(-t/T_1) - \exp(-t/T_2)\right] \quad ...(4.8)$$

The chopped waveforms are generated by the following system of equations:

$$E(t) = \begin{cases} E_1 \left[\exp(-t/T_1) - \exp(-t/T_2)\right], & t<T \quad ...(4.9.a) \\ E(T_c) - 1000(t-T_c), & T_c<t<T_z \quad ...(4.9.b) \\ F(t)\sin[3.124(t-T_z)], & t>T_z \quad ...(4.9.c) \end{cases}$$

where T is the time to chopping and:

$$T_z = T_c + E(T_c)/1000 \quad ....(4.10)$$

$$F(t) = -0.4\exp[-(t+T_z)/0.8] \qquad .....(4.11)$$

E_1 in Eqs.(4.8) and (4.9.a) represents a constant which is adjusted in order to obtain a waveform of the desired maximum amplitude, E_{max} . The ratio E_1/E_{max} can be determined from the expression for the maximum amplitude of the function given by Eq.(4.8). The parameters of the input waveforms used during the simulation are given in Tab.4.4.

TABLE 4.4

Parameters of the input waveforms

waveform type	E_{max} [kV]	T_1 [μs]	T_2 [μs]	T_c [μs]	
				front	tail
1.2/50	1300	68.2	.405	1	7
250/2500	1300	3155	62.5	-	-

4.5 Analysis of Numerical Accuracy

The purpose of this analysis was to determine the combinations of steps Δt and Δx which satisfy the stability condition and yield numerical results of acceptable accuracy for the shortest possible computational time, known as CPU (Central Processor Unit) time. The influence of these two steps on the accuracy was examined in examples involving the

line of geometry shown in Fig.4.3. In each case, the line was subjected to 450kV positive voltage impulses of the 1.2/50 μs and the 250/2500 μs types.

It was noted that higher values of Δt and Δx, which also satisfy the stability condition, produce high-frequency oscillations around the crest value of the computed voltage waveforms, and that amplitude of these oscillations decreases as the magnitudes of the steps decrease. Furthermore, in the examples with the line energized with zero steady-state voltage, it was noted that similar oscillations appear around the knee which corresponds to the point of transition to corona conditions, causing an error in the inception voltage. When the line, energized with zero steady-state voltage, was subjected to a 1.2/50 μs voltage impulse, the influence of steps Δt and Δx on numerical accuracy was found to be the strongest. This was the situation when the rate of rise of the computed voltages was the highest. The effect that Δt and Δx have on the corona inception voltage can be seen from Fig.4.4. The waveforms in this figure are computed when the non-energized line under consideration was subjected to a 450 kV, 1.2/50 μs positive voltage impulse. The waveforms were computed at distances of 0.6, 1.2, and 2.4 km from the beginning of the line. The influence of these two steps on numerical accuracy was also examined in the example when the line under consideration, energized with 450 kV, was subjected to a positive , 450 kV, 250/2500 μs voltage impulse.

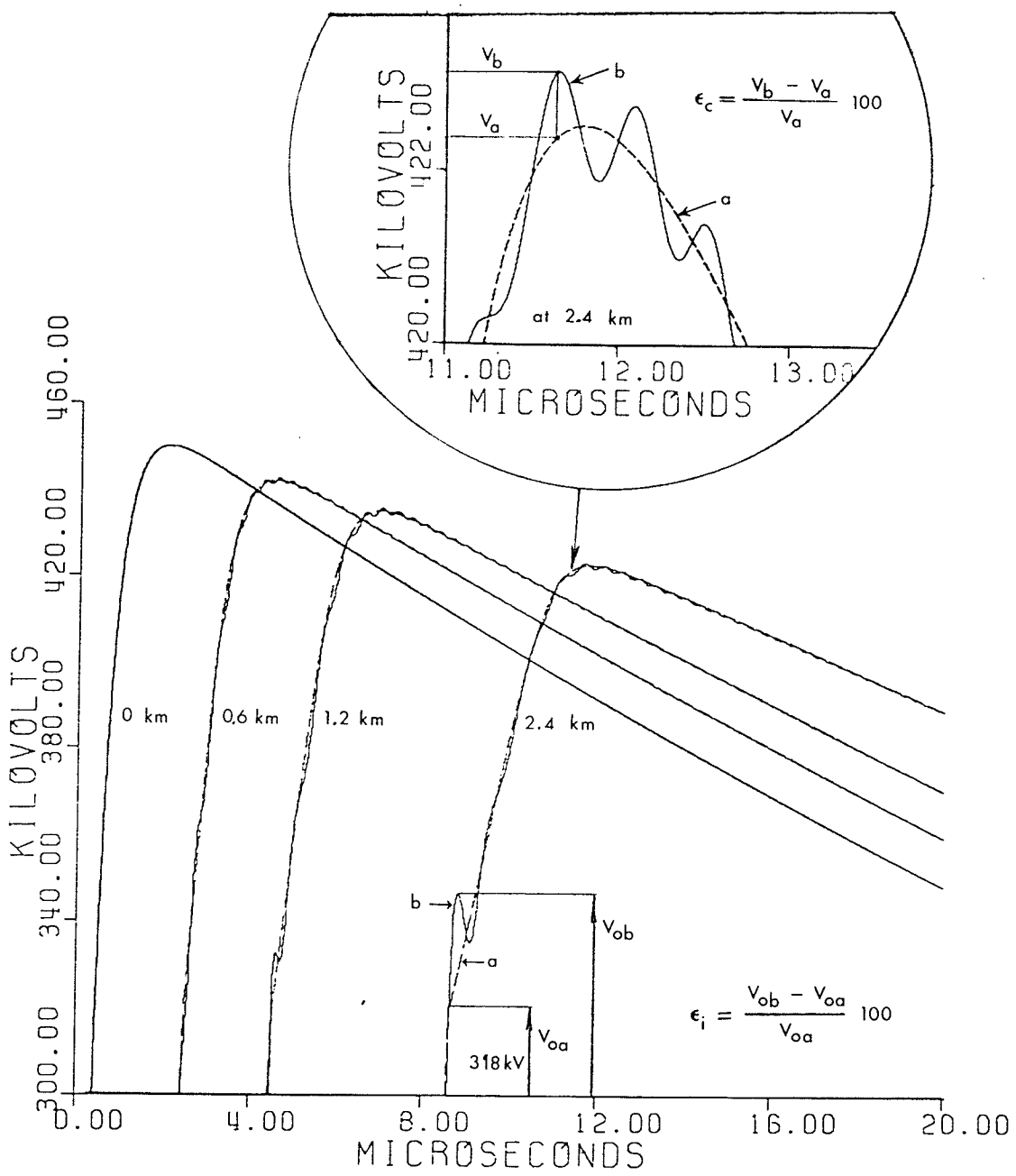

Figure 4.4: Influence of different values of Δt and Δx on V_0 . a) base waveform. b) Δt=0.02 μs, Δx=0.02 km.

The values of Δt and Δx were varied in two ranges, and they are given in Tab.4.5, along with the values for the stability factor, CPU time, and computed errors. When

TABLE 4.5

Numerical errors caused by variation of time and displacement steps

Δt [μs]	Δx [km]	Stability factor -	CPU time [s]	Error [%] ϵ_c	Error [%] ϵ_i
Impulse 1.2/50 μs, V_{SS} =0, x=2.4 km					
0.01	0.003	0.979	70.51	0.000	0.50
0.01	0.006	0.490	36.00	0.009	6.30
0.01	0.010	0.293	22.13	0.020	7.20
0.02	0.006	0.979	17.64	0.060	3.60
0.02	0.010	0.587	11.53	0.090	7.80
0.02	0.020	0.293	6.17	0.186	8.30
0.02	0.030	0.196	4.49	0.329	13.40
0.04	0.012	0.979	4.94	0.201	4.32
Impulse 250/2500 μs, V_{SS} =450 kV, x=240 km					
10	5	0.587	4.80	0.000	-
10	10	0.293	2.84	0.035	-
20	6	0.979	2.38	0.058	-
20	10	0.587	1.70	0.088	-
40	12	0.979	0.82	0.197	-

propagation of a lightning-type voltage impulse was simulated, a waveform computed with Δt=0.01 μs and Δx=0.003 km was chosen as a basis for error computation. This waveform satisfies two conditions. First, it exhibits no high-frequency oscillations around crest; second, the point of transition to corona occurs at the voltage which is almost equal to the value calculated by Eq.(4.5). Similarly, when propagation of a switching-type voltage impulse was simulated, the waveform computed with Δt=10 μs and Δx=5 km was chosen as a basis for error computation,

since it satisfies the same conditions. For all the examples, the error was computed in the region around the crest, as a maximum relative error between the base waveform and the waveforms computed with different steps Δt and Δx, as shown in Fig.4.4. This error is denoted as ϵ_c . In cases where the line was energized with zero steady-state voltage, the relative error in the inception voltage was computed too, and it is denoted by ϵ_i .

From Tab.4.5 and Fig.4.4, it can be concluded that the error effect due to different steps Δt and Δx, is much more pronounced at the point of transition to corona conditions than around the crest value of a computed voltage waveform. The results in Tab.4.5 also indicate that the high-frequency oscillations are of smaller amplitude if displacement step, Δx, is chosen as a distance slightly greater than that travelled by the wave for time Δt. If this condition is satisfied, the performance of the FDM can be significantly accelerated. It should be noted that, in such a case, the stability factor is almost equal to 1. Some researchers[10,14] did not pay enough attention to this condition.

Since the main purpose of this study is the analysis of the effect that corona has on attenuation and distortion of overvoltage waves on HVDC transmission lines, the error ϵ_c is considered to be of prime importance in the analysis of numerical accuracy. In this case, the error of ϵ_c =0.2% was

considered permissible. Therefore, the values of $\Delta t=0.04$ μs and $\Delta x=0.012$ km were chosen for the simulations involving the lightning-type voltage impulses, and $\Delta t=40$ μs and $\Delta x=12$ km for those involving the switching-type impulses. These values show that, with the FDM, a very god description of a standard lightning voltage impulse can be obtained with not less than 30 points in the region of its front. For a standard switching impulse, number of points in the region of the front should not be less then 6.

4.6 Description of Simulation Cases

Based upon the value and polarity of the steady-state voltage, the following two cases were considered:

Case 1: Steady-State Voltage, V_{SS} = +450 kV

Here, the line energized with +450 kV was subjected to 450 kV lightning and switching type positive voltage impulses. When the line was subjected to lightning-type voltage impulses, the voltages were computed at distances of 0.6 km, 1.2 km, and 2.4 km from the beginning of the line. When a switching-type impulse was applied at the beginning of the line, the voltages were computed at distances of 60 km, 120 km, and 240 km. For each of the computed voltages, values of the maximum amplitude and attenuation were computed and they are given in Tabs.4.6-4.9. The waveforms obtained in this example are shown in Figs.4.5-4.8.

Case 2: Steady-State Voltage of the Line, V_{SS} = 0 kV

In this case, the line was considered to be non-energized. The types of voltage impulses and the respective distances on the line, where the voltages were computed, were the same as in Case 1. The values of the maximum amplitude and attenuation for each of the computed voltages are given in Tabs.4.10-4.12. The waveforms obtained in this example are shown in Figs.4.9-4.11.

4.7 Analysis of the Results of the Simulation

It can be noted that, in the cases where the line is not energized, Figs.3.9-3.11, the waveforms are characterized by a sudden change of the slope in the region of the front, which results in the characteristic knee on the diagrams. This point on the diagrams corresponds to the moment of transition from non-corona conditions to impulse corona conditions. The voltage which corresponds to this point is the corona inception voltage. When the line is energized (Figs.4.5-4.8), the knee does not appear because corona already existed during the steady-state (Assumption 2, section 4.1). According to the results in Tabs.4.6-4.12, the attenuation in this case, is the highest. It should be also noted that in all simulated examples, the rate of attenuation decreases as a surge propagates along the line and that this decrease is nonlinear.

It is interesting to analyze the propagation of a full and chopped voltage impulse of the same type. Tabs.4.10 and 4.12 show the results for the attenuation of a 450 kV, full 1.2/50 μs, and a 450 kV 1.2/50 μs chopped at the tail positive voltage impulse, respectively. It can be noted that both impulses are equally attenuated. This result may appear surprising since the chopped impulse dissipates less energy during corona than the corresponding full one, and therefore expected to be less attenuated. However, the chopped impulse is an impulse that also has a lower energy level than the corresponding full one. The degree of attenuation of an impulse due to corona, depends on the amount of energy dissipated by corona relative to the total energy of the unattenuated impulse, rather than on the absolute amount of the dissipated energy, alone. Realistically, chopped impulses should be even more attenuated than the corresponding full ones because of the skin effect which is very pronounced for this kind of voltage impulse.

The values of the maximum amplitudes given in Tabs.4.6.-4.12, indicate that the highest overvoltages can be expected when an energized line is subjected to a voltage impulse of the same polarity as the steady-state voltage. When the line was subjected to a full lightning-type voltage impulse, the maximum amplitude of the line voltage decreased from 2 p.u. to 1.75 p.u. after the impulse propagated a distance of only 2.4 km, Tab.4.6. This result indicates

that lightning-type overvoltage surges can be dangerous for a substation only for lightning strokes intercepted by a line at a distance from the substation which is comparable to those in the simulation example.

The results of the simulation with a switching-type voltage impulse, Tab.4.9, show that the maximum amplitude of the line voltage decreased from 2 p.u. to 1.67 p.u. after the impulse propagated a distance of 240 km. Considering that the switching-type overvoltage surges on present HVDC transmission lines have to propagate the distances in the order of several hundred kilometers, this type of overvoltage surges can be considered to be even less dangerous than those resulting from lightning strokes.

TABLE 4.6

Computed attenuation of a full 450 kV, 1.2/50 μs positive voltage impulse

STEADY-STATE VOLTAGE: V = 450 kV				
LOCATION	MAXIMUM VOLTAGE AMPLITUDE		ATTENUATION	
km	kV	p.u.	%	db
0.0	899.99	2.00	0.	0.
0.6	867.72	1.93	7.2	-0.32
1.2	838.85	1.86	13.6	-0.63
2.4	789.60	1.75	24.5	-1.22

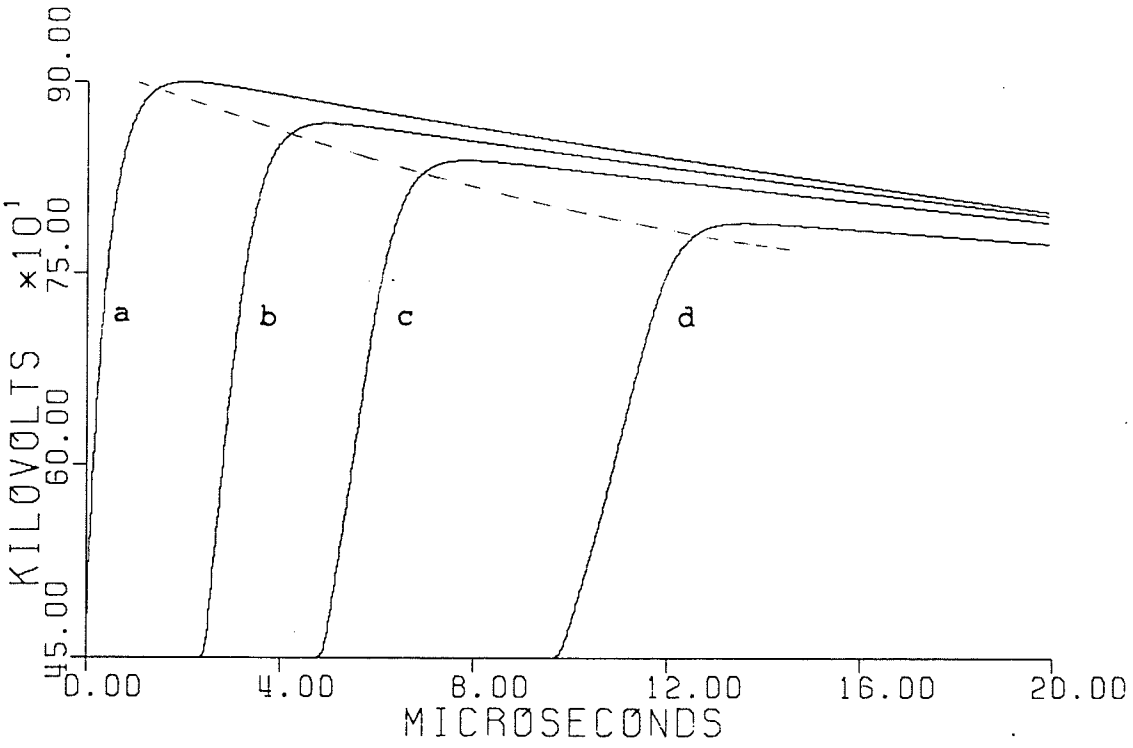

Figure 4.5: Propagation of a positive 450 kV, 1.2/50 μs voltage impulse along the line energized with 450kV. a) 0 km, b) 0.6 km, c) 1.2 km, d) 2.4 km

TABLE 4.7

Computed attenuation of a 450 kV, 1.2/50 μs positive voltage impulse chopped on the front

STEADY-STATE VOLTAGE: V_{SS} = 450 kV				
LOCATION	MAXIMUM VOLTAGE AMPLITUDE		ATTENUATION	
km	kV	p.u.	%	db
0.0	870.46	1.93	0.	0.
0.6	832.76	1.85	9.0	-0.41
1.2	805.06	1.79	15.6	-0.73
2.4	759.04	1.69	26.5	-1.34

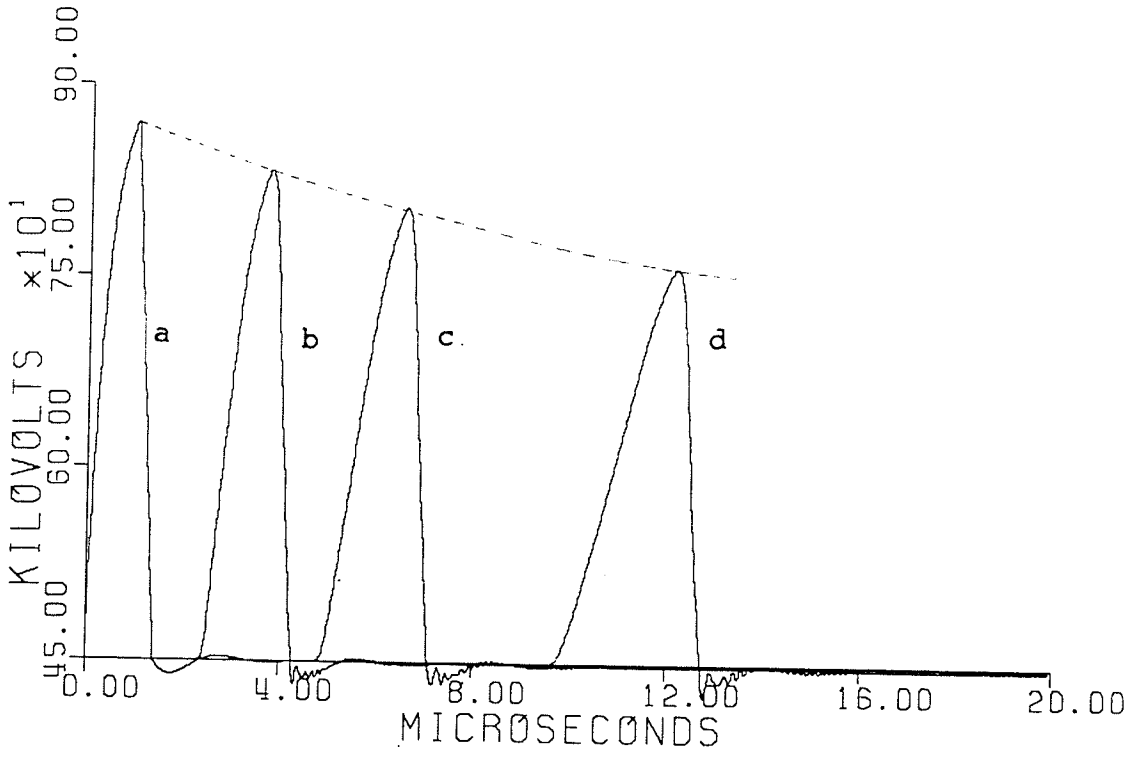

Figure 4.6: Propagation of a 450 kV, 1.2/50 μs positive voltage impulse chopped at the front, along the line energized with 450 kV. a) 0 km, b) 0.6 km, c) 1.2 km, d) 2.4 km

TABLE 4.8

Computed attenuation of a 450 kV, 1.2/50 μs positive voltage impulse chopped at the tail

STEADY-STATE VOLTAGE: V_{SS} = 450 kV				
LOCATION	MAXIMUM VOLTAGE AMPLITUDE		ATTENUATION	
km	kV	p.u.	%	db
0.0	899.99	2.00	0.	0.
0.6	867.71	1.93	7.2	-0.32
1.2	838.84	1.86	13.6	-0.63
1.8	789.59	1.75	24.5	-1.22

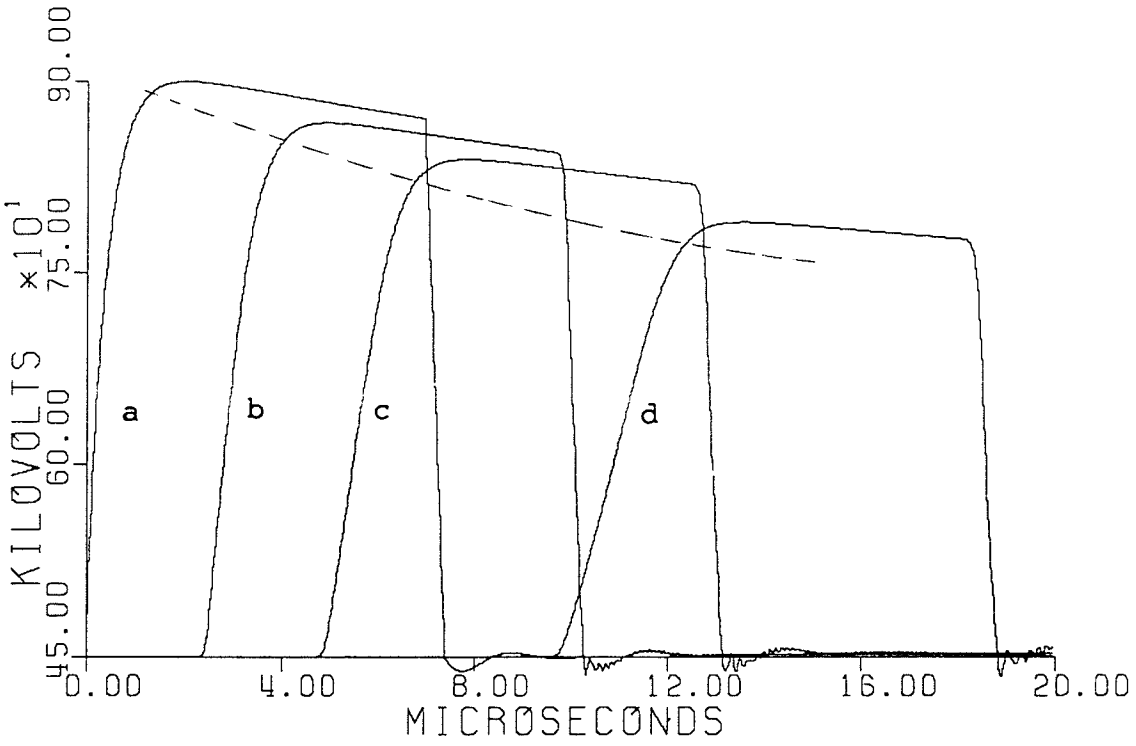

Figure 4.7: Propagation of a 450 kV, 1.2/50 μs positive voltage impulse chopped at the tail, along the line energized with 450 kV. a) 0 km, b) 0.6 km, c) 1.2 km, d) 2.4 km

TABLE 4.9

Computed attenuation of a 450 kV, 250/2500 positive voltage impulse

STEADY-STATE VOLTAGE: V_{SS} = 450 kV				
LOCATION	MAXIMUM VOLTAGE AMPLITUDE		ATTENUATION	
km	kV	p.u.	%	db
0.0	899.99	2.00	0.	0.
60	855.26	1.90	9.9	-0.45
120	816.24	1.81	18.6	-0.89
240	753.25	1.67	32.6	-1.71

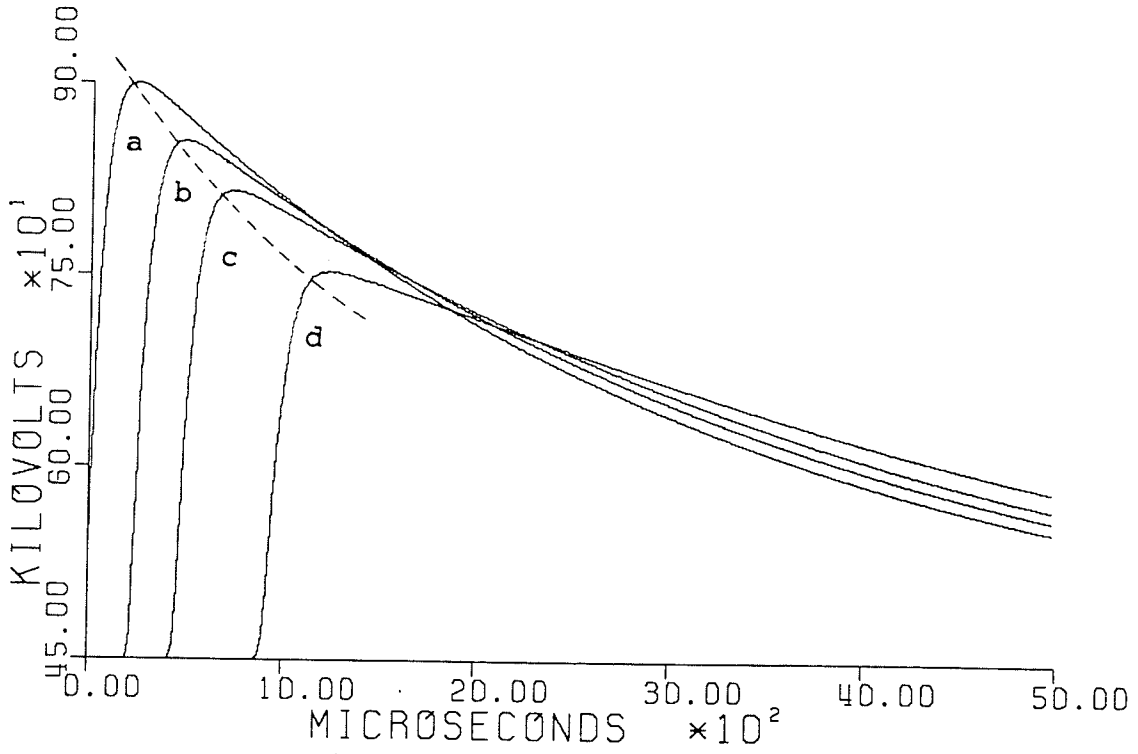

Figure 4.8: Propagation of a 450 kV, 250/2500 μs positive voltage impulse along the line energized with 450 kV. a) 0 km, b) 60 km, c) 120 km, d) 240 km

TABLE 4.10

Computed attenuation of a full 450 kV, 1.2/50 μs positive voltage impulse

STEADY-STATE VOLTAGE: V_{SS} = 0.0 kV				
LOCATION	MAXIMUM VOLTAGE AMPLITUDE		ATTENUATION	
km	kV	p.u.	%	db
0.0	449.99	1.00	0.	0.
0.6	442.05	0.98	1.8	-0.08
1.2	434.89	0.96	3.4	-0.15
2.4	422.49	0.94	6.1	-0.27

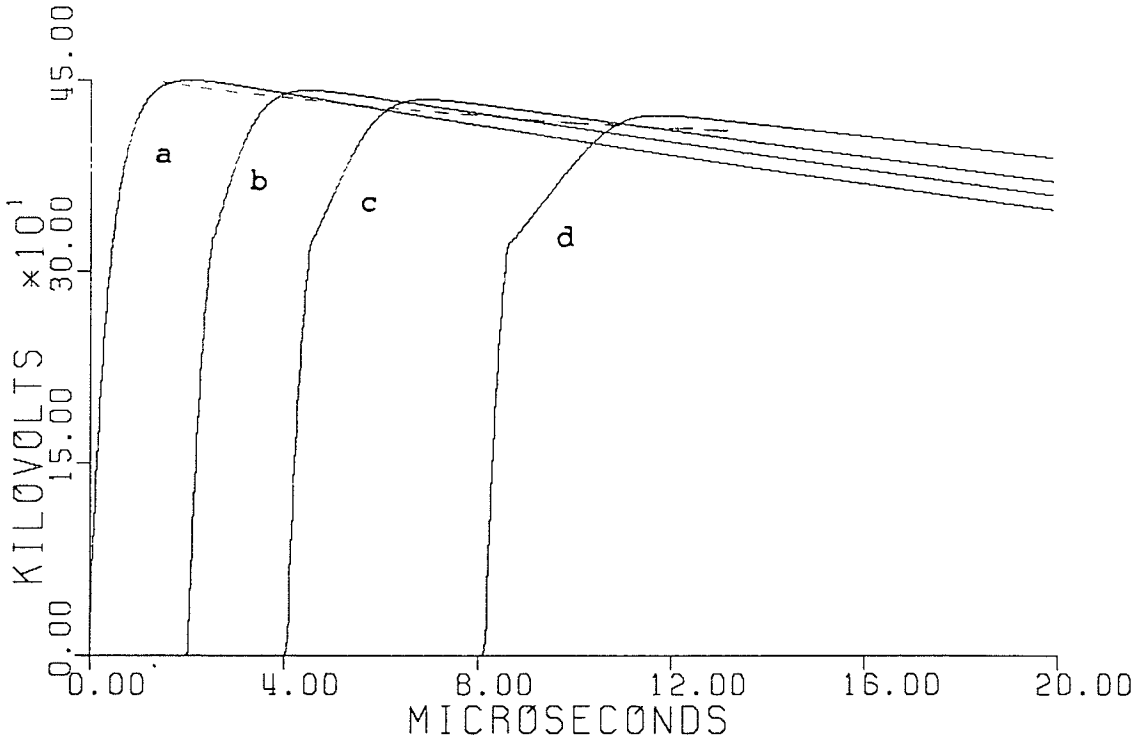

Figure 4.9: Propagation of a positive 450 kV, 1.2/50 μs voltage impulse along the non-energized line. a) 0 km, b) 0.6 km, c) 1.2 km, d) 2.4 km. V_0 =318 kV.

TABLE 4.11

computed attenuation of a 450 kV, 1.2/50 μs positive voltage impulse chopped on the front

STEADY-STATE VOLTAGE: V_{SS} = 0.0 kV				
LOCATION	MAXIMUM VOLTAGE AMPLITUDE		ATTENUATION	
km	kV	p.u.	%	db
0.0	420.45	0.93	0.	0.
0.6	409.74	0.91	2.5	-0.11
1.2	404.09	0.89	3.9	-0.17
2.4	395.35	0.88	6.0	-0.27

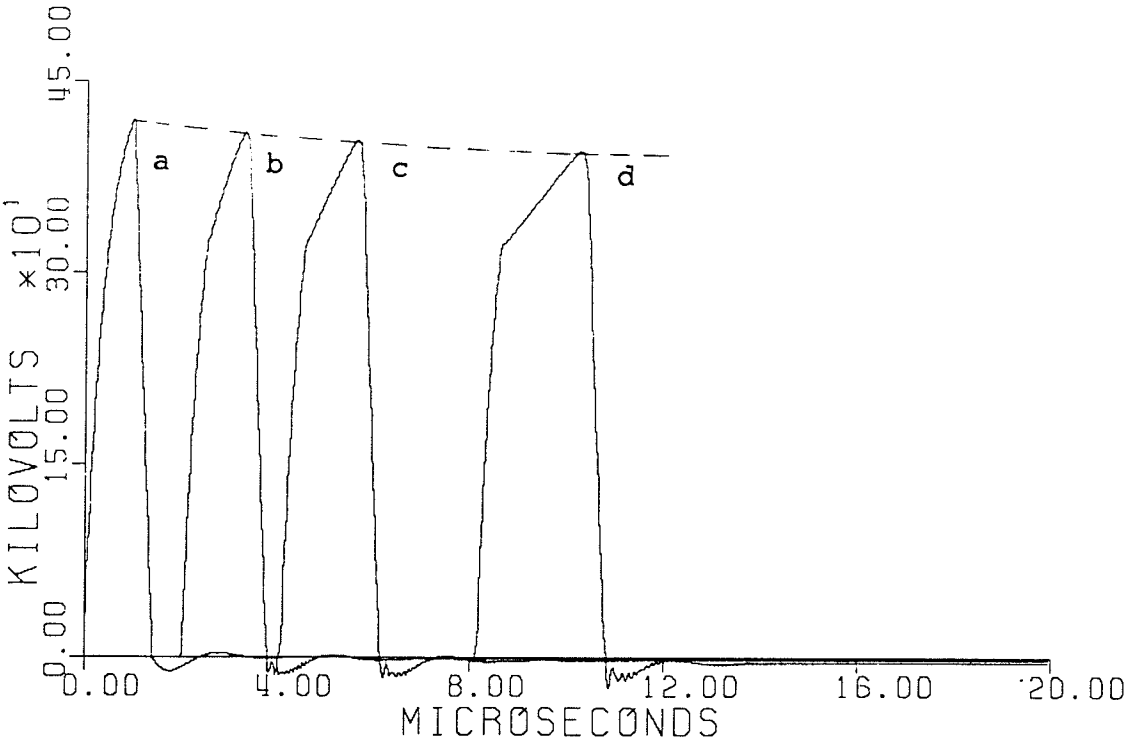

Figure 4.10: Propagation of a 450 kV, 1.2/50 μs positive voltage impulse chopped at the front, along the non-energized line. a) 0 km, b) 0.6 km, c) 1.2 km, d) 2.4 km. V_0 = 318 kV

TABLE 4.12

Computed attenuation of a positive 450 kV, 1.2/50 μs chopped at the tail

STEADY-STATE VOLTAGE: V_{SS} = 0.0 kV				
LOCATION	MAXIMUM VOLTAGE AMPLITUDE		ATTENUATION	
km	kV	p.u.	%	db
0.0	449.99	1.00	0.	0.0
0.6	442.05	0.98	1.8	-0.08
1.2	434.89	0.96	3.4	-0.15
2.4	422.49	0.94	6.1	-0.27

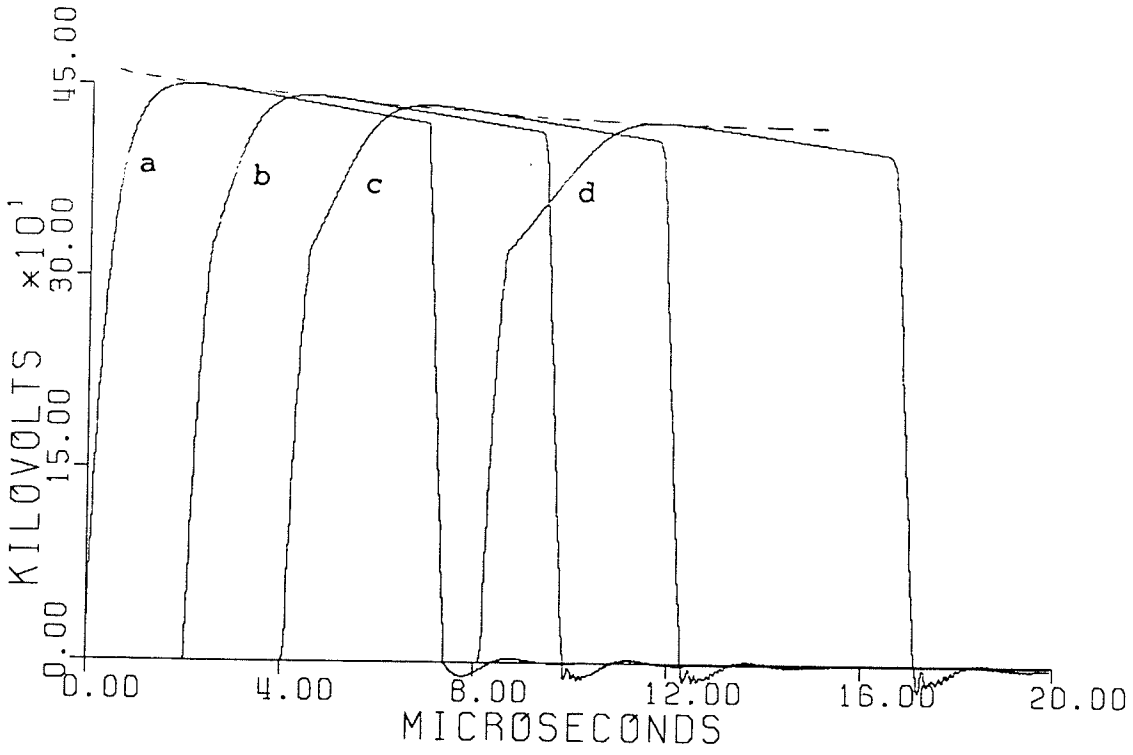

Figure 4.11: Propagation of a 450 kV, 1.2/50 μs positive voltage impulse chopped at the tail, along the non-energized line. a) 0 km, b) 0.6 km, c) 1.2 km, d) 2.4 km. V_0 = 318 kV.

4.8 Description of the Program

Based on the system of TLE given by Eqs. (2.40) a computer program was developed to simulate the propagation of overvoltage surges along semi-infinite HVDC monopolar transmission lines. The program consists of a main program where the values of currents and voltages are computed for given time and displacement, and three subroutines which generate different input voltage waveforms and the coefficients A, B, C, and D, Eqs.(2.41). The flowchart of the main program is shown in Fig.4.12.

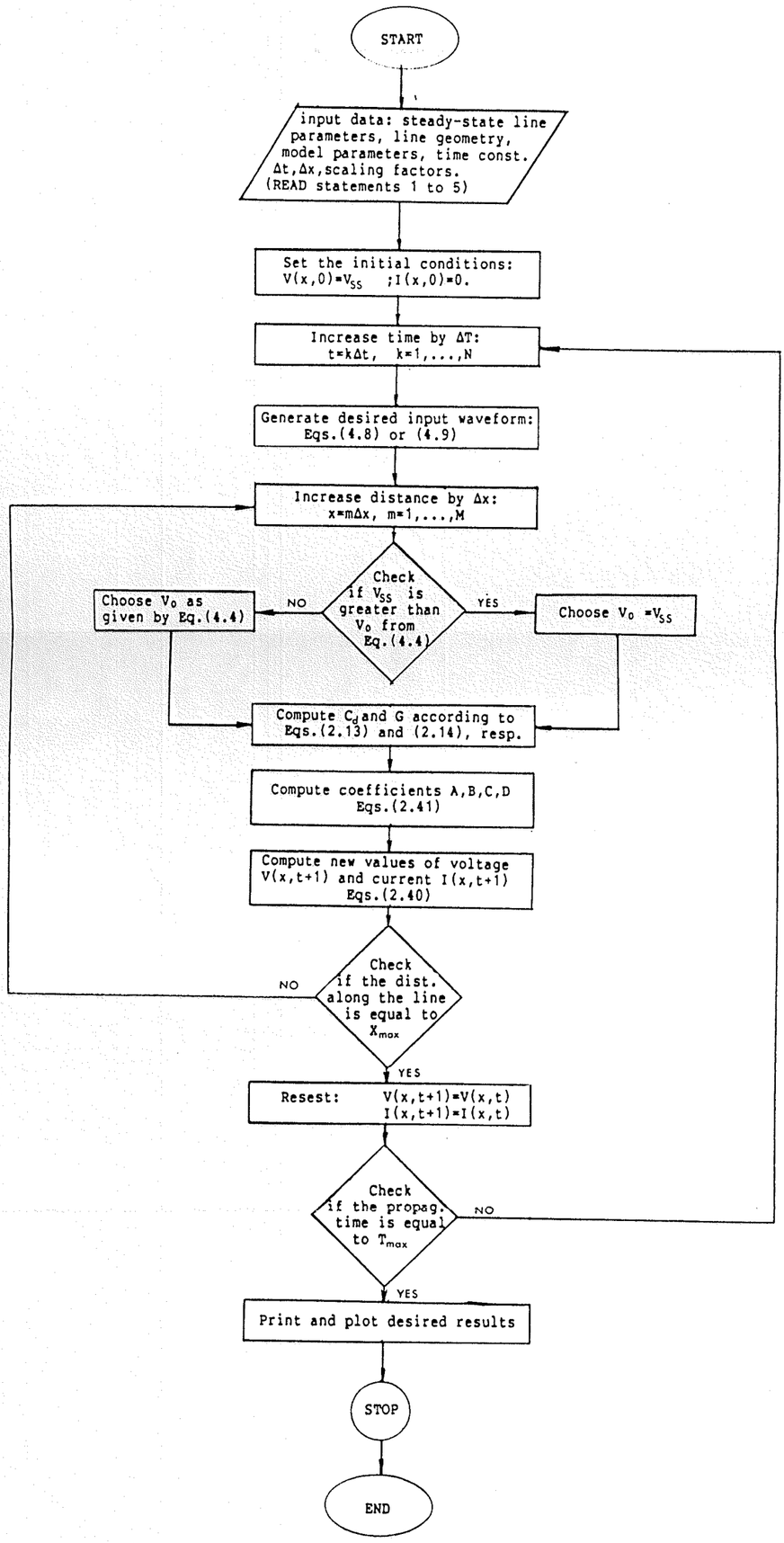

Figure 4.12: Flowchart of the main program

The program starts with reading the input data, arranged through the following READ statements:

READ statement 1: ($T_1, T_2, T_c, E_{max}, V_0, V_{SS}$, ITYPE)

The first three parameters are time constants specified in microseconds and they define the shape of the input voltage impulse. Thus, the constants T_1 and T_2 represent the constants for double exponential form and the constant T_c represents the time for chopping. The parameters E_{max}, V_0, V_{SS} are voltage parameters with the values specified in kilovolts. They represent the maximum amplitude of the input voltage impulse, the corona inception voltage, and the steady-state operating voltage of the line, respectively. The parameter V_0 is specified as a positive value only. This implies that both positive and negative corona start at the same voltage which is just an approximation whose influence on the final result is negligible. The parameter ITYPE specifies the type of an input waveform. It has a form of an integer whose value can be either 0 or 1, which denote:

ITYPE = 0, Full input waveform of the lightning or switching-type.

ITYPE = 1, Chopped input waveform of the lightning or switching-type.

READ statement 2: ($X_{max}, \Delta x, \Delta t, T_{max}$)

The first two parameters are spatial parameters specified in kilometers and they define the length of the line and the displacement step Δx, respectively. The second two parameters are time parameters specified in microseconds and they define the time step and the maximum time of propagation ,respectively. The maximum propagation time is determined from the value for X_{max} and the actual speed of propagation.

READ statement 3: (R,L,C_0,σ_1,σ_2,a ,h)

These parameters represent the transmission line parameters. Thus,

R = transmission line resistance,[Ω/km]. This study was carried out with R=0,

L = transmission line inductance [H/km],

C_0= geometric capacitance of the line [F/km],

σ_2 = corona loss constant [dimensionless],

σ_1 = another corona loss constant [dimensionless],

a = equivalent radius (GMR) of a conductor bundle [m].

If the ratio between the spacing and a subconductor diameter is greater than 10, the bundling effect can be neglected. In such cases, this parameter should have the value of the equivalent radius of a

subconductor. This approximation is valid for the Nelson River conductor bundle configuration.

h = average suspension height [m].

READ statement 4: (NX1,NX2,NX3,IPR)

The first three parameters are integer parameters and they define the location on the line where the voltage waveforms are to be computed. They represent the number of displacement steps Δx from the beginning of the line up to the desired locations on the line. This program enables a choice of three such locations. Parameter IPR specifies a printing option related to printing the output results. It has the form of a positive integer where:

IPR = 0, The values of maximum voltage amplitudes and the attenuation are printed only. The values of the voltage amplitudes are expressed in kilovolts and in units relative to the value of the steady-state voltage, V_{SS} . The attenuation is expressed in percent and in decibels.

IPR > 0, The complete waveforms at desired locations will be obtained in a printed

form. This option also includes the option obtained for IPR = 0.

READ statement 5: (XBEG,YBEG,XDIV,XNDIV,YDIV,YNDIV)

These parameters are scaling parameters and are related to plotting of the output results. The parameters have the following meaning:

XBEG = starting value on the time-axis, [μs]

YBEG = starting value on the voltage-axis, [kV]

XDIV = scaling factor for the time-axis, [μs/div]

XNDIV = number of divisions on the time-axis, [div] (1 division = 1 in.)

YDIV = scaling factor for the voltage-axis, [kV/div]

YNDIV = number of divisions on the voltage-axis, [div] (1 division = 1 in.)

After setting the initial conditions, a voltage impulse of the desired type is generated at the beginning of the line, in accordance to Eqs.(4.8) or (4.9). During each time step, the voltages and the currents are computed all along the line. At each location the values of the computed voltages are compared with the values of either the inception voltage or the steady-state voltage and the coefficients A, B, C, and D, Eqs.(2.41) computed accordingly. When the maximum propagation time is exceeded,

the computed values of the line voltage at the desired locations are printed and/or plotted, depending on the specified value of parameter IPR.

The coefficients A, B, C, and D are computed in a subroutine nameds PAR. Whenever the new values of these coefficients are to be computed, this subroutine is invoked from the main program.

The input voltage impulses are generated by two subroutines. A subroutine named SWLSUR generates full lightning or switching-type voltage impulses according to Eq.(4.8), whereas a subroutine named CHPSUR generates the chopped voltage impulses according to Eqs.(4.9).

The limitation of this program is determined by the number of time steps Δt, chosen for computation. This number is determined by the ratio $T_{max}/\Delta t$ and not more than 2000 such steps can be used with this program.

5. CONCLUSION AND SUGGESTIONS FOR FURTHER RESEARCH

The purpose of this study was to highlight the influence that impulse corona has on overvoltage surges which propagate along monopolar HVDC transmission lines, and to indicate an optimal technique for modelling this phenomenon.

In Chapter 3, the performances of three, already existing, corona models are compared. These models are based on two approaches to corona modelling which are the most applicable for the HVDC environment.

One approach is based on approximation of Q-V loops experimentally recorded for different conductor bundle configurations, weather conditions, and different shapes and polarity of applied voltage impulses. Although different approximation techniques are used by different authors, the idea is the same - to develop the expressions which approximate experimental Q-V loops in order to render them valid for a range of different line geometries, and voltage polarities and waveshapes. Such loops are usually dependent on at least two empirical constants which accommodate the change of the Q-V loop shape in different practical situations. Since the area enclosed by the loop is proportional to the energy dissipated by corona, this kind

of modelling technique results in exclusion of a conductance term from the TLE. In this study, the models utilizing this approach are classified as Q-V loop models.

The other approach is based on analytical approximation of only that part of an experimental Q-V loop where the first derivative is positive. Corona losses, however, are accommodated by an appropriate conductance G, derived from one of the existing corona loss laws. This approach, too, is dependent on empirical constants which, generally speaking, determine the rates of capacitance increase and the energy dissipation during corona. In this study, the models utilizing this approach to corona modelling are classified as conductance models.

The main disadvantage of both approaches is their dependance on empirical constants. Modelling techniques that do not use such constants are available in the literature. However, they are developed for application in HVAC transmission systems only.

The results of the comparison study carried out in Chapter 2, represent the main contribution of this thesis. These results clearly indicate that the conductance model, with the conductance G determined from Peek's law for steady-state corona losses, yields the most accurate results of all the compared models. In addition to this, it is a very simple model and has high practical applicability.

Because of these reasons, the conductance model is recommended for implementation on HVDC transmission lines.

The implementation of this model on a monopolar HVDC transmission line, Chapter 4, necessitated the determination of a set of values for the two empirical constants used in the model, which are valid for switching-type voltage impulses. These values (Tab.4.3) are determined for the Nelson River conductor bundle configuration, positive voltage impulses, and a fair weather condition. The extension of the conductance model for this class of voltage waveforms and therefore its application for an energized monopolar transmission line, represents another contribution of this thesis.

As a part of the implementation, the FDM used as a numerical procedure in this study, is optimized through an analysis of numerical accuracy, which is also carried out in Chapter 4. The results for CPU time, and the numerical errors presented in Tab.4.5, indicate that the value of the stability factor should be maintained slightly less, or if possible, equal to 1. If the time and displacements steps are chosen in accordance with this condition, the performance of the FDM can be significantly accelerated, without sacrificing the accuracy of computation very much. For example, with $\Delta t=0.04\ \mu s$ and $\Delta x=0.012$ km, the CPU time is more than seven times shorter than that obtained with the combination of Δt and Δx used by Inoue, while the numerical error remained as small as 0.2%.

The conductance model implementation is concluded with a numerical simulation of transient behaviour of the line considered in this study, and it was carried out with a practical range of input voltage waveshapes. The results of the simulation presented in Chapter 4, indicate that the influence of corona on the attenuation of both lightning and switching surges is very strong. In other words, it acts as if the surge arresters were placed all along the line, and therefore, provides an additional level of surge protection on these lines. This implies that the analyses of overvoltage transient phenomena on HVDC transmission lines, with the inclusion of the corona effect, may result in reduced insulation level of equipment connected to the line.

The corona model considered in this study is based on experimental results obtained for positive voltage impulses of the lightning and switching-type. Unfortunately, experimental results for negative voltage impulses are not available in the literature and therefore the utilization of this model for this kind of voltage impulses was not possible at this time. Furthermore, the model proposed in this study does not take skin effect into account, which also contributes to additional attenuation and distortion of the overvoltage surges. Therefore, further improvements of this model are necessary and the following is suggested:

1. Utilization of the model for negative voltage impulses. This is particularly important for the analyses involving the lightning-type voltage

impulses, since the most of direct lightning strokes result in negative voltage surges. This will be possible only when experimental results for this kind of voltage impulse become available.

2. A more general program which includes both the skin effect and corona should be created. Since the skin effect is a frequency-dependent phenomenon, it is suggested that the modelling of both corona and the skin effect should be done in the frequency-domain.
3. The research has to be extended to include modelling of corona on bipolar HVDC transmission lines. In this case the pole-to-ground and the pole-to-pole capacitances will both be nonlinear functions of voltage and, therefore, it is expected that the overvoltage surges will be even more attenuated and distorted than those on the monopolar lines.

The results presented in Chapter 4 of this study, as well as research done in the past, indicate that a certain level of steady-state corona should be allowed in HVDC transmission systems in order to obtain an additional level of overvoltage protection and, therefore, reduce the associated investments. On the other hand, steady-state corona produces power losses which transmission line designers tend to minimize. It becomes obvious that, in order to determine the permissible level of steady-state corona, an optimization study which will take into account

the cost of power losses due to corona on one side, and the reduction of investments for the surge protection on the other side, must be done in the near future.

LIST OF REFERENCES

[1] Peek F.W, Dielectric Phenomena in High Voltage Engineering, New York, London: McGraw-Hill Inc., 1929.

[2] Electrical Power Research Institute Transmission Line Reference Book HVDC to +600 kV, Palo Alto, California: Boneville Power Administration

[3] Kuffel E., Zaengl W.S. High Voltage Engineering, Pergamon Press, 1984.

[4] Isaacson E., Keller H.B. Analysis of Numerical Methods, John Willey and Sons, 1966.

[5] Ryan H.J, Henline H.H. Hysteresis Character of Corona Formation, Trans. AIEE, Vol.43, October 1924, pp.1118-1124.

[6] Skilling H.H., Dykes P. Distortion of Traveling Waves by Corona, Trans. AIEE, Vol.56, July 1937, pp.850-837.

[7] Wagner C.F., Loyd B.L. Effects of Corona on Traveling Waves, Trans. AIEE, Vol.PAS-74, October 1955, pp.858-872

[8] Maruvada P.S., Menemenlis H., Malewski R. Corona Characteristics of Conductor Bundles Under Impulse Voltages, Trans. IEEE, Vol.PAS-96, No.1, Jan./Feb. 1977, pp.102-115.

[9] Afgani M., Harrington R.J. Charge Model for Studying Corona on Overhead Transmission Lines, Proc. IEE, Vol.130, Pt.C, No.1, January 1983, pp.16-21.

[10] Lee K.C. Nonlinear Corona Models in an Electromagnetic Transient Program (EMTP), Trans. IEEE, Vol.PAS-102, No.9, September 1983, pp.2936-2942.

[11] Gary C., Timotin A., Cristescu D. Prediction of Surge Propagation Influenced by Corona and Skin Effect, Proc. IEE, Vol.130, Pt.A, No.5, July 1983, pp.264-272.

[12] Ovick N.L., Kusic G.L. Including Corona Effect for Traveling Waves on Transmission Lines, Trans. IEEE, Vol.PAS-103, No.12, December 1984, pp.-3643-3649.

[13] Abdel-Salam M., Abdel-Sattar S. Negative Corona Inception as Influenced by Steepness of Applied Impulse Waves, Gaseous Dielectrics IV, p.370-375, edited by Christophorou L.G. and Pace M.O., Pergamon Press, May 1984.

[14] Inoue A. Propagation Analysis of Overvoltage Surges with Corona Based Upon Charge Versus Voltage Curve, Trans. IEEE, Vol.PAS-104, No.3, March 1985, pp.655-660.

[15] Semlyen A., Wei-Gang H. Corona Modelling for the Calculation of Transients on Transmission Lines, Trans. IEEE, Vol.PWRD-1, No.3, July 1986, pp.228-238.

Appendix A

PROGRAM FOR THE SIMULATION OF CORONA-AFFECTED VOLTAGE SURGE PROPAGATION ALONG MONOPOLAR TRANSMISSION LINES

```
      SUBROUTINE PAR
      REAL*8 A,B,C,D
      COMMON A,B,C,D,R,XL,CDYN,G,DX,DT
      A=1.-G*DT*1.D-6/CDYN
      B=DT*1.D-6/(CDYN*DX)
      C=1.-R*DT*1.D-6/XL
      D=DT*1.D-6/(XL*DX)
      RETURN
      END
      SUBROUTINE CHPSUR(K)
      REAL*8 T(2100),E(2100)
      COMMON /W/ T,E,E0,T1,T2,TC
      EKSP=(EXP(-ALOG(T2/T1)/(1-T1/T2))
     &      -EXP(-ALOG(T2/T1)/(T2/T1-1)))
      EA=E0/EKSP
      IF(T(K+1).GE.TC) GO TO 1
      E(K+1)=EA*(DEXP(-T(K+1)/T1)-DEXP(-T(K+1)/T2))
      EN=E(K+1)
      GO TO 3
1     E(K+1)=EN-1000.*(T(K+1)-TC)
      IF(E(K+1).LE.0.) GO TO 2
      GO TO 3
```

```
2      TCE=EN/1000.+TC
       E(K+1)=-.04*EA*DEXP(-(T(K+1)-TCE)/.80)
      &        *DSIN(3.124*(T(K+1)-TCE))
3      CONTINUE
       RETURN
       END
       SUBROUTINE SWLSUR(K)
       REAL*8 T(2100),E(2100)
       COMMON /W/ T,E,E0,T1,T2
      EKSP=(EXP(-ALOG(T2/T1)/(1-T1/T2))
     &      -EXP(-ALOG(T2/T1)/(T2/T1-1)))
       EA=E0/EKSP
       TCTRL=(T(K+1))/T2
       EP1=DEXP(-T(K+1)/T1)
       IF(TCTRL.GE.180.) GO TO 1
       EP2=DEXP(-T(K+1)/T2)
       GO TO 2
1      EP2=0.
2      E(K+1)=EA*(EP1-EP2)
       RETURN
       END
       REAL*8 T(2100),E(2100),VK1(2000),VK(2000),
      &       SK1(2000),SK(2000)
       REAL*8 A,B,C,D
       REAL VSS,VSWCH,VCOR,SG,RC,H
       DIMENSION IBUF(4000),YARRAY(2002),
      &          XARRAY(2002),VOLT(2000,4),
      &          VMAX(2000),DIST(4),VMX(4),
```

```
     &          VMPU(4),ATTN(4),ATDB(4)
      COMMON A,B,C,D,R,XL,CDYN,G,DX,DT
      COMMON /W/ T,E,E0,T1,T2,TC
      READ *,T1,T2,TC,E0,VCOR,VSS,ITYPE
      READ *,XMAX,DX,DT,TMAX
      READ *,R0,XL,C0,SG,SC,RC,H
      READ *,NX1,NX2,NX3,IPR
      READ *,XBEG,YBEG,XDIV,XNDIV,YDIV,YNDIV
      NX=XMAX/DX
      NT=TMAX/DT
      VSWCH=VCOR
      IF(ABS(VSS).GE.VCOR) VSWCH=ABS(VSS)
      QC=SC*SQRT(.5*RC/H)*1.D-8
      QG=SG*SQRT(.5*RC/H)*1.D-8
      C1=C0+2*QC*(1.-VCOR/VSWCH)
      G1=QG*(1.-VCOR/VSWCH)**2
      DO 50 I=1,NX
      VK(I)=VSS
      SK(I)=0.
      VMAX(I)=VK(I)
50    CONTINUE
      EMAX=0.
      DO 1000 K=1,NT
      R=R0
      T(K+1)=K*DT
      IF(ITYPE.GT.1) GO TO 2000
      IF(ITYPE.EQ.0) CALL SWLSUR(K)
      IF(ITYPE.EQ.1) CALL CHPSUR(K)
```

```
      IF(ABS(EMAX).GT.DABS(E(K))) GO TO 51
      EMAX=E(K)
51    CONTINUE
      IF (DABS(VK(1)).GE.VSWCH) GO TO 1
      IF(ITYPE.EQ.1
     &   .AND.DABS(VK(1)).LT.ABS(VMAX(1))) GO TO 3
      GO TO 2
1     IF(ITYPE.EQ.1) GO TO 3
      CDYN=C0+2*QC*(1.-VCOR/DABS(VK(1)))
      G=QG*(1.-VCOR/DABS(VK(1)))**2
      CALL PAR
      GO TO 4
2     CDYN=C1
      G=G1
      CALL PAR
      GO TO 4
3     CDYN=C0+2*QC*(1.-VCOR/ABS(VMAX(1)))
      G=QG*(1.-VCOR/ABS(VMAX(1)))**2
      CALL PAR
4     VK1(1)=A*VK(1)-B*(SK(2)-SK(1))
      SK1(1)=C*SK(1)-D*(VK1(1)-E(K))
      IF(DABS(SK1(1)).LE.1.D-70) SK1(1)=0.
      IF(DABS(VK1(1)).LE.1.D-70) VK1(1)=0.
      IF(ABS(VMAX(1)).GT.DABS(VK1(1))) GO TO 45
      VMAX(1)=VK1(1)
45    CONTINUE
      DO 200 I=2,NX
      IF(DABS(VK(I)).GE.VSWCH) GO TO 5
```

```
      IF(ITYPE.EQ.1
     &   .AND.DABS(VK(I)).LT.ABS(VMAX(I))) GO TO 7
      GO TO 6
5     IF(ITYPE.EQ.1) GO TO 7
      CDYN=C0+2*QC*(1.-VCOR/DABS(VK(I)))
      G=QG*(1.-VCOR/DABS(VK(I)))**2
      CALL PAR
      GO TO 8
6     CDYN=C1
      G=G1
      CALL PAR
      GO TO 8
7     CDYN=C0+2*QC*(1.-VCOR/ABS(VMAX(I)))
      G=QG*(1.-VCOR/ABS(VMAX(I)))**2
      CALL PAR
8     VK1(I)=A*VK(I)-B*(SK(I+1)-SK(I))
      SK1(I)=C*SK(I)-D*(VK1(I)-VK1(I-1))
      IF(DABS(SK1(I)).LE.1.D-70) SK1(I)=0.
      IF(DABS(VK1(I)).LE.1.D-70) VK1(I)=0.
      IF(ABS(VMAX(I)).GT.DABS(VK1(I))) GO TO 200
      VMAX(I)=VK1(I)
200   CONTINUE
      VOLT(K,1)=E(K)
      VOLT(K,2)=VK1(NX1)
      VOLT(K,3)=VK1(NX2)
      VOLT(K,4)=VK1(NX3)
      DO 300 I=1,NX
      VK(I)=VK1(I)
```

```
      SK(I)=SK1(I)
300   CONTINUE
1000  CONTINUE
      VMX(1)=EMAX
      VMX(2)=VMAX(NX1)
      VMX(3)=VMAX(NX2)
      VMX(4)=VMAX(NX3)
      DO 1100 ISZ=1,4
      ATTN(ISZ)=100.*(1.-VMX(ISZ)/VMX(1))
      ATDB(ISZ)=10.*ALOG10(VMX(ISZ))/VMX(1))
      IF(VSS.EQ.0.) GO TO 1100
      VMPU(ISZ)=ABS(VMX(ISZ)/VSS)
1100  CONTINUE
      DIST(2)=DX*NX1
      DIST(3)=DX*NX2
      DIST(4)=DX*NX3
      WRITE(6,9) (DIST(I),VMX(I),VMPU(I),
     &            ATTN(I),ATDB(I),I=1,4)
9     FORMAT(8X,'X=',F8.4,1X,'KM',3X,'VMAX=',F12.5,1X,
     &      'KV (',F4.2,1X,'P.U.)',3X,'ATTN=',F4.1,1X,
     &      'PER CENT=',F7.2,'DB')
      WRITE(6,10) VSS
10    FORMAT(24X,1X,'VSS=',F12.5,1X,'KV')
      IF(IPR.EQ.0) GO TO 1200
      WRITE(6,11)(T(K),VOLT(K,1),VOLT(K,2),VOLT(K,3),
     &            VOLT(K,4),K=1,NT)
11    FORMAT(//,(1X,'T=',F8.4,4X,'E=',F10.4,4X,
     *      'V=',F12.6,4X,'V=',F12.6,4X,'V=',F12.6))
```

```
C     -- PLOTING ROUTINE --
1200  CALL AREA(8.25,10.75)
      CALL PLOTS(IBUF,4000)
      CALL PLOT(1.5,1.5,-3)
      XARRAY(2001)=XBEG
      XARRAY(2002)=XDIV
      YARRAY(2001)=YBEG
      YARRAY(2002)=YDIV
      CALL AXIS(0.,0.,'MICROSECONDS',-12,XNDIV,0.0,
     &          XARRAY(2001),XARRAY(2002))
      CALL AXIS(0.,0.,'KILOVOLTS',9,YNDIV,90.,
     &          YARRAY(2001),YARRAY(2002))
      DO 500 L=1,4
      DO 400 I=1,2000
      XARRAY(I+1)=T(I)
      IF(XARRAY(I+1).LT.XBEG) XARRAY(I+1)=XBEG
      YARRAY(I)=VOLT(I,L)
      IF(YARRAY(I).LT.YBEG) YARRAY(I)=YBEG
400   CONTINUE
      XARRAY(2001)=XBEG
      XARRAY(2002)=XDIV
      YARRAY(2001)=YBEG
      YARRAY(2002)=YDIV
      CALL LINE(XARRAY,YARRAY,2000,1,0,0)
500   CONTINUE
      CALL PLOT(0.,0.,999)
      CALL PLOT(0.,0.,9999)
      GO TO 2100
```

```
2000  WRITE(6,15)
15    FORMAT(1X,'ERROR - UNKNOWN TYPE OF INPUT SIGNAL')
2100  CONTINUE
      STOP
      END
```